

Bridging Boundaries: $T\bar{T}$, Double Holography, and Reflected Entropy

Debarshi Basu,^{a,b} Himanshu Chourasiya,^b Ankur Dey,^b and Vinayak Raj^{b,c}

^a*Shing-Tung Yau Center and School of Physics, Southeast University,
Nanjing 210096, China*

^b*Department of Physics, Indian Institute of Technology,
Kanpur 208016, India*

^c*School of Science, Huzhou University,
Huzhou 313000, Zhejiang, China*

E-mail: debarshi.128@gmail.com, chim@iitk.ac.in, ankurd21@iitk.ac.in,
vinayak.hep.th@gmail.com

ABSTRACT: We investigate the reflected entropy for bipartite mixed state configurations in a $T\bar{T}$ deformed boundary conformal field theory in 2 dimensions (BCFT₂). The bulk dual is described by asymptotically AdS₃ geometries with the cut off surface pushed deeper into the bulk and truncated by an end of the world brane. We obtain the reflected entropy up to a linear order in the radial cut-off for static and time dependent configurations involving an eternal black hole, from the island and defect extremal surface (DES) prescriptions in the context of the deformed AdS/BCFT. We observe agreement of the leading order correction for all cases between the two prescriptions. We also obtain the analogous of the Page curves for the reflected entropy and investigate the modification due to the $T\bar{T}$ deformation.

Contents

1	Introduction	2
2	Review	4
2.1	$T\bar{T}$ deformed CFT	4
2.2	AdS ₃ /BCFT ₂ and defect extremal surface	5
2.3	Holographic $T\bar{T}$ with a boundary	6
2.4	Entanglement entropy	7
2.5	Reflected entropy	9
2.6	Island and DES formula for Reflected entropy	10
3	Zero Temperature	10
3.1	Disjoint Subsystems	11
3.1.1	Entanglement Entropy phase-1	11
3.1.2	Entanglement Entropy phase 2	13
3.2	Adjacent Subsystems	19
3.2.1	Entanglement Entropy Phase:1	19
3.2.2	Entanglement Entropy Phase:2	20
4	Time dependent reflected entropy in black hole evaporation	24
4.1	The emergence of a 2d eternal black hole	24
4.2	Reflected entropy between black hole interiors	26
4.2.1	Entanglement Entropy Phase: 1	26
4.2.2	Entanglement Entropy Phase: 2	28
4.3	Reflected entropy between black hole interior and radiation	30
4.3.1	The Entanglement entropy phase	30
4.3.2	Reflected Entropy Phase: 1	32
4.3.3	Reflected Entropy Phase: 2	32
4.4	Reflected entropy between radiation subsystems	34
4.4.1	Entanglement Entropy Phase: 1	34
4.4.2	Entanglement Entropy Phase: 2	36
4.5	Page curve	37
5	Conclusions	40
A	On geodesics in cut-off AdS₃	41
A.1	Geodesic on a constant τ -slice	41
A.2	Geodesic on a constant x -slice	42

1 Introduction

The black hole information loss problem has been a central topic of research for several decades, spurring significant progress in semi-classical and quantum gravity. Recent studies have made impactful strides towards resolving this problem through the *island* framework that provide access to regions inside black hole geometries at late times [1–6]. Through this framework, the Page Curve [7–9] for the von Neumann entropy of the Hawking radiation was reproduced for a CFT coupled to a theory of gravity by including the “island” inside the gravitational region in the entanglement wedge of the radiation bath. The emergence of these islands, is attributed to the late time dominance of *replica wormhole* saddles in the gravitational path integral for the Rényi entanglement entropy. The so called island formula was inspired by the quantum extremal surface (QES) prescription [10] which describes the quantum corrections to the holographic entanglement entropy [11–14].

A more elegant and insightful interpretation of the island formula may be provided by the *double holography* framework [1, 14–26]. This involves considering the CFT_d coupled to the semiclassical gravity to be holographic and be described by a $(d + 1)$ -dimensional gravity theory. In the literature, this higher dimensional picture have been termed as the bulk description for the original setup which is termed as the brane description. This gravity-plus-matter system in the brane description may, in turn be described through a quantum mechanical system residing on the boundary of the CFT_d which was dubbed as the boundary description. In this double holographic setup, the computation of the entanglement entropy through the island formula in the brane description translates to its holographic characterization through the Ryu-Takayanagi (RT) prescription in the bulk AdS_{d+1} geometry.

Diverging from the above, boundary conformal field theories (BCFTs) [15, 27–30], defined as CFTs on a manifold with a boundary, have garnered significant interest in recent years. The holographic dual to a BCFT_2 is described by an asymptotically AdS_3 spacetime bounded by an end-of-the-world (EOW) brane with Neumann boundary conditions. The holographic entanglement entropy formula [28, 29] for this framework involves modification of the homology condition to incorporate extremal surfaces anchored to the EOW brane as well. In [31], the authors explore an extension of this $\text{AdS}_3/\text{BCFT}_2$ duality, where the Neumann boundary condition on the EOW brane is modified by addition of *defect* conformal matter.¹ The works [31, 32] introduce the defect extremal surface (DES) formula which extends the RT prescription by incorporating contributions from defect matter fields in the context of defect $\text{AdS}_3/\text{BCFT}_2$. Notably, the DES formula in this defect $\text{AdS}_3/\text{BCFT}_2$ has been proposed and verified as the doubly holographic counterpart of the island formula in the lower dimensional effective description.²

¹The term “defect matter” refers to degrees of freedom that are localized on a defect, a lower dimensional submanifold, within the full spacetime.

²Note that in [31–35], the brane perspective described in the double holographic framework has been termed as the *lower dimensional effective description* as the authors obtained the brane perspective through partial dimensional reduction of the bulk AdS_3 geometry with the EOW brane. We will use these two terminologies interchangeably in this article.

While entanglement entropy is a suitable metric for investigating the entanglement structure of bipartite pure states, it fails to accurately characterize the mixed state entanglement structure. For systems involving bipartite mixed states, it is preferable to utilize alternative (computable) measures such as reflected entropy [36, 37], entanglement negativity [38, 39], entanglement of purification [40, 41], and balanced partial entanglement entropy [42]. These measures offer a more nuanced characterization of the complex entanglement structure in mixed states.

While the original island framework was primarily developed for pure states, many physically relevant situations—such as subsystems within the Hawking radiation or black holes coupled to non-isolated environments—often lead to mixed states. As stated above, in such scenarios, it becomes imperative to generalize the island framework to accommodate mixed states, enabling a more detailed description of entanglement structures in gravitational settings. The authors in [43, 44] provided this generalization in terms of the reflected entropy [36, 45]. Reflected entropy is based on canonical purification of the given mixed state and is described holographically in terms of the area of the bulk entanglement wedge cross-section (EWCS) [40, 41]. Subsequently, in [33], a DES formula for the reflected entropy was forwarded which was shown to be the bulk counterpart of the island formula for the reflected entropy in the defect $\text{AdS}_3/\text{BCFT}_2$ scenario.³ This equivalence provides a robust framework for studying the entanglement in mixed states within these holographic settings.

Motivated by the desire to test the robustness of the island framework for the reflected entropy and its doubly holographic generalizations, it is imperative to investigate them in less conventional gravitational settings. In this context, CFTs deformed by an irrelevant operator composed of the stress-energy tensor [47–49] provide a fertile testing ground due to their solvable nature. These irrelevant deformations introduce a finite cutoff in the dual AdS_3 geometries [50] satisfying Dirichlet boundary conditions,⁴ which have been studied extensively in the literature [52, 56–80]. We here consider such deformations of BCFTs which provide a natural toy model to investigate the island formalism. The dual AdS geometry with an EOW brane now also involves a finite cut-off, which adds subtlety to the standard AdS/BCFT correspondence and demands a careful analysis. While the island formula and its reflected entropy analogue have been primarily studied in standard asymptotically AdS spacetimes, it is not a priori clear whether their structure survives in such geometries with finite radial cutoff and modified boundary conditions. Investigating mixed state entanglement in such setups, particularly through computable measures like reflected entropy, therefore provides a test and extends the applicability of the island paradigm in a more intricate setting.

The two kind of boundaries discussed earlier, namely the EOW brane in the context of AdS/BCFT, and the asymptotic boundary at the finite cut-off surfaces in holographic

³Similar DES formulas for entanglement negativity were also forwarded in [34, 35] which provide double holographic description for the island formula for the entanglement negativity [46].

⁴Note that alternative proposals for the holographic duality of these $T\bar{T}$ deformed theories have also been proposed in the literature, such as [51–55]. It is expected that they will coincide under certain limits, however the exact matching for general cases remains a non-trivial open issue.

dual of $T\bar{T}$ deformed theories, have very different nature because of distinct boundary conditions governing them. In order to elucidate these differences, the authors in [81, 82] investigated a spacetime with both of these boundaries. In order to have a transparent boundary between the two surfaces, they introduced the same matter field on the EOW as is present at the asymptotic boundary in the dual picture. In the boundary description, this corresponds to a $T\bar{T}$ deformation of a BCFT₂, which may be obtained through a partial dimensional reduction of a braneworld gravity theory glued to a non-conformal bath with $T\bar{T}$ deformation [81]. The authors investigated the entanglement structure of bipartite pure states in such a model through the entanglement entropy.

The above advancements underscore the importance of characterizing mixed state entanglement in AdS geometries that incorporate both an EOW brane and a finite radial cut-off surface. To this end, we utilize the reflected entropy to study bipartite mixed states in asymptotically AdS₃ geometries with a finite radial cut-off, which originates from $T\bar{T}$ deformation, and is truncated by an EOW brane. We utilize the DES formula for the reflected entropy to compute bulk reflected entropy through the EWCS and compare these with island computation in the lower dimensional effective description. Additionally, we extend our analysis to time-dependent configurations, involving black hole and radiation subsystems in an effective lower-dimensional theory.

The remainder of this article is structured as follows. In section 2, we briefly review various aspects of $T\bar{T}$ deformation, reflected entropy, and the island and DES formulas that are essential for computing reflected entropy. In section 3, we introduce the DES formula for calculating reflected entropy in asymptotically AdS₃ geometries with a finite radial cut-off bounded by an EOW brane. We compute the reflected entropy for both adjacent and disjoint intervals, considering various possible entanglement entropy phases in a static time slice, and demonstrate the equivalence of the DES and the island formula. In section 4, we extend our analysis to time-dependent configurations. We start by reviewing the essentials of the eternal black hole in the two-dimensional effective picture, followed by describing the DES and island computations for the reflected entropy between interior regions of the black hole, between the black hole and radiation in the bath system, and between radiation subsystems. Finally, we summarize our findings in section 5.

2 Review

2.1 $T\bar{T}$ deformed CFT

In this subsection we review the $T\bar{T}$ deformation in CFTs and its holographic dual. Consider 2d conformal field theory in a flat space given by the metric $ds^2 = -dt^2 + dx^2$. $T\bar{T}$ deformation of such a CFT₂ is defined by [48, 49]

$$\frac{dI_{QFT}^{(\mu)}}{d\mu} = -2\pi \int d^2x (T\bar{T})_\mu, \quad I_{QFT}^{(\mu)} \Big|_{\mu=0} = I_{CFT}, \quad (2.1)$$

where I is the Lorentzian action and μ is the deformation parameter. $(T\bar{T})$ is the $T\bar{T}$ deformation operator, which is defined in terms of the components of the stress energy

tensor T^{ab} as

$$(T\bar{T}) = \frac{1}{8} \left(T_{ab}T^{ab} - (T_a^a)^2 \right). \quad (2.2)$$

The author in [47] have shown that the $T\bar{T}$ operator satisfies the factorization formula

$$\langle T\bar{T} \rangle = \frac{1}{8} \left(\langle T_{ab} \rangle \langle T^{ab} \rangle - \langle T_a^a \rangle^2 \right). \quad (2.3)$$

In the bulk picture, the authors in [50, 65] have proposed the $T\bar{T}$ deformed CFT_2 in flat space to be dual to a quantum gravity in AdS_3 with a radial cut-off

$$ds^2 = \frac{\ell^2}{z^2} (-dt^2 + dx^2 + dz^2), \quad z > z_c, \quad (2.4)$$

where Dirichlet boundary conditions are imposed at $z = z_c$. The deformation parameter is related to the radial cut-off as [65]

$$\mu = \frac{8G_N}{\ell} z_c^2 = \frac{12}{c} z_c^2. \quad (2.5)$$

2.2 $\text{AdS}_3/\text{BCFT}_2$ and defect extremal surface

In this subsection, we briefly review the $\text{AdS}_3/\text{BCFT}_2$ correspondence, proposed in [28, 29]. A boundary conformal field theory (BCFT) is a conformal field theory (CFT) defined on a manifold \mathcal{M} with boundary $\partial\mathcal{M}$, where conformal boundary conditions are specified. It was shown in [27] that the holographic dual of a BCFT is given by an asymptotically AdS spacetime \mathcal{N} truncated by an end-of-world (EOW) brane \mathcal{Q} on which the Neumann boundary condition is imposed. The bulk action is given by [28, 29]

$$I_0 = -\frac{1}{16\pi G_N} \int_{\mathcal{N}} \sqrt{g}(R - 2\Lambda) - \frac{1}{8\pi G_N} \int_{\mathcal{Q}} \sqrt{h}(K - (d-1)T). \quad (2.6)$$

Here K represents the trace of the extrinsic curvature on the EOW brane with tension T . By varying the above action with respect to the induced metric on the brane h_{ab} , we can determine the brane trajectory, which consequently leads to the Neumann boundary conditions

$$K_{ab} = (K - T)h_{ab}. \quad (2.7)$$

The $\text{AdS}_3/\text{BCFT}_2$ framework was further extended in [31, 32] by incorporating conformal matter (essentially a two-dimensional CFT) on a tensionless EOW brane, which consequently induces a finite tension. As a result, the brane moves to a position with constant angle. The corresponding bulk action in this setup is given by

$$I = I_0 + \int_{\mathcal{Q}} \sqrt{h} \mathcal{L}_{\mathcal{Q}} \quad (2.8)$$

where $\mathcal{L}_{\mathcal{Q}}$ corresponds to the Lagrangian of a CFT_2 with large central charge; typical examples may be cooked up in terms a large number of massless scalar fields or in terms of

the Liouville action [17]. The Neumann boundary condition (2.7) is modified through the expectation value of the stress tensor of this conformal matter theory as [28, 31, 32]

$$K_{ab} = (K - T)h_{ab} + 8\pi G_N \langle T_{ab} \rangle \quad , \quad \langle T_{ab} \rangle = \frac{2}{\sqrt{h}} \frac{\partial \mathcal{L}_Q}{\partial h_{ab}} \quad (2.9)$$

and the EOW brane is essentially treated as a defect in the bulk geometry⁵.

In the modified bulk scenario with defect conformal matter on the EOW brane, the entanglement entropy of an interval in the original BCFT includes contributions from the defect matter. This leads to a modification of the usual Ryu-Takayanagi (RT) formula to the defect extremal surface (DES) formula as

$$S_{\text{DES}} = \min \text{ext}_{\Gamma_A, X} \left\{ \frac{\text{Area}[\Gamma_A]}{4G_N} + S_{\text{defect}}(D) \right\}, \quad X = \Gamma_A \cap D, \quad (2.10)$$

where Γ_A is the RT surface and D is the defect region along the EOW brane as depicted in fig. 1.

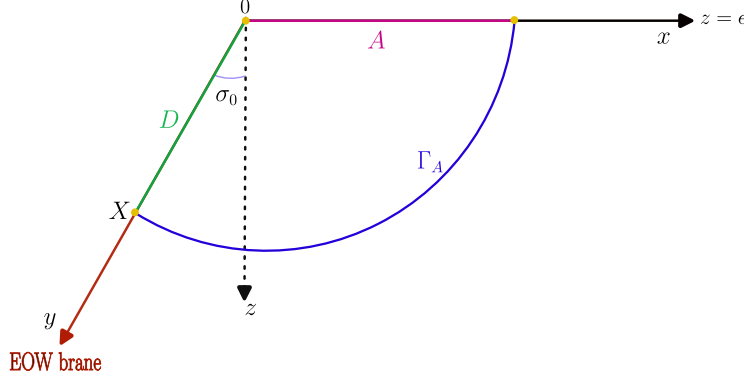


Figure 1: Schematics of the defect extremal surface for the EE of a subsystem A .

2.3 Holographic $T\bar{T}$ with a boundary

A $T\bar{T}$ deformed theory with a boundary can be realized by ensuring that the deformed theory preserves a space-time Z_2 symmetry with a fixed point at $x = 0$ which corresponds to a tensionless brane in the holographic bulk. The holographic dual of a $T\bar{T}$ deformed CFT_2 in flat space with a boundary is still given by AdS_3 with a radial cut-off at $z = z_c$ and the introduction of the Z_2 quotient modifies the bulk metric as

$$ds^2 = \frac{\ell^2}{z^2} (-dt^2 + dx^2 + dz^2), \quad z > z_c, \quad x \geq 0. \quad (2.11)$$

⁵Note that since the EOW brane has an AdS_2 profile, which is maximally symmetric, the stress tensor expectation value in the defect CFT_2 is proportional to induced metric h_{ab} and only affects the tension on the EOW brane. In this sense, the CFT_2 degrees of freedom on the EOW brane do not really act as dynamical fields backreacting on the ambient geometry, and the EOW brane may be treated as a lower dimensional defect.

As stated in [30, 83], such a metric is equivalent to considering a tensionless EOW brane at $x = 0$. In the bulk, the EOW brane starts from $z = z_c$ as the boundary of the Z_2 quotient $T\bar{T}$ deformed CFT₂ moves from $z = \epsilon$ to $z = z_c$. Under the bulk coordinate transformation

$$x = -y \tanh \frac{\sigma}{\ell}, \quad z = z_c + y \operatorname{sech} \frac{\sigma}{\ell}, \quad (2.12)$$

the metric eq. (2.11) becomes,

$$ds^2 = \frac{\ell^2}{(z_c + y \operatorname{sech} \frac{\sigma}{\ell})^2} \left(-dt^2 + dy^2 + \frac{y^2 \operatorname{sech} \frac{\sigma}{\ell}}{\ell^2} d\sigma^2 \right). \quad (2.13)$$

Assume that the EOW brane is located at $\sigma = \sigma_0$. Now solving the Neumann boundary condition on the EOW brane, one can easily find the relation between tension T and brane location as

$$T = \frac{\tanh \frac{\sigma_0}{\ell}}{\ell}. \quad (2.14)$$

The metric induced on the brane may be written as follows

$$ds^2 = \Omega(y)^2 (-dt^2 + dy^2), \quad (2.15)$$

where $\Omega(y) = \frac{\ell}{(z_c + y \operatorname{sech} \frac{\sigma_0}{\ell})}$ is the conformal factor. As described in [31], the tensionless brane is orthogonal to the asymptotic boundary and if we add the conformal matter on the brane, it turns to a finite tension and moves to a position with a constant σ angle. To impose transparent boundary conditions for the $T\bar{T}$ deformed bath, we include the same field theory on the EOW brane with an identical deformation parameter to that of the $T\bar{T}$ -deformed CFT on the cut-off boundary. This modified the Neumann boundary condition on the EOW brane is given by eq. (2.9)

On inclusion of matter in the bulk : It is important to emphasize that incorporating conformal matter localized on the EOW brane does not require the introduction of additional sources in the holographic dictionary [31]. Rather, the conformal matter acts as a modification to the boundary conditions placed at the conformal boundary $x = 0$ [81]. As described in [81], the new EOW brane is still along the constant σ_0 slice with tension $T = \frac{1}{\ell}$. The conformal matter is placed on the EOW brane in order to obtain a lower dimensional effective theory more suited to the island paradigm, where one requires the same quantum field theory to reside on the entire hybrid manifold. Furthermore, as the inclusion of such matter theory does not backreact on the ambient geometry, it is safely assumed that cut-off prescription for the holographic dual of $T\bar{T}$ -deformed CFTs is still applicable in the large N approximation [81].

2.4 Entanglement entropy

In this subsection, we will briefly review the computation of the EE between a subsystem $A = [0, L]$ and its complement in the above setup, both from the bulk (DES) and island perspective.

DES formula:

Consider a subsystem $A = [0, L]$ in the bath region with a boundary, the generalized entropy is given as

$$\begin{aligned}
S_{\text{gen}}(a) &= S_{\text{RT}}(-a, L) + S_{\text{brane matter}}(a), \\
&= \frac{c}{6} \cosh^{-1} \left(\frac{(L + a \tanh \frac{\sigma_0}{\ell})^2 + (z_c + a \operatorname{sech} \frac{\sigma_0}{\ell})^2 + z_c^2}{2z_c(z_c + a \operatorname{sech} \frac{\sigma_0}{\ell})} \right) \\
&\quad + \frac{c}{6} \log \frac{2a\ell}{(z_c + a \operatorname{sech} \frac{\sigma_0}{\ell})\epsilon_y},
\end{aligned} \tag{2.16}$$

where the first term is the usual RT surface length between point (L, z_c) and $(-a \tanh \frac{\sigma_0}{\ell}, z_c + a \operatorname{sech} \frac{\sigma_0}{\ell})$ and second term is the EE of the quantum matter on the defect brane. Here a is the boundary position of island and ϵ_y is the UV cut-off for the $T\bar{T}$ deformed CFT on the brane. Now extremizing the above expression over a we get the extremal value of a

$$a = L - 2e^{\frac{\sigma_0}{\ell}} z_c + \mathcal{O}(z_c^2), \tag{2.17}$$

Substituting a into S_{gen} we obtain the EE for subsystem A from the DES formula as

$$S_{\text{DES}} = \frac{1}{4G_N} \left(\frac{\sigma_0}{\ell} + \log \left[\frac{2\ell \cosh \frac{\sigma_0}{\ell}}{\epsilon_y} \right] + \log \frac{2L}{z_c} - \frac{e^{\frac{\sigma_0}{\ell}}}{L} z_c \right) + \mathcal{O}(z_c^2). \tag{2.18}$$

Boundary island formula:

We now describe the lower-dimensional effective theory for the above bulk configuration, where the island formula is applicable. This can be achieved through a combination of a partial Randall-Sundrum reduction [84, 85] *i.e.*, doing dimensional reduction for the wedge between EOW brane and tensionless brane and the usual AdS/CFT duality [86] for the rest of the bulk. As described in [31–33], this procedure involves dividing the AdS_3 bulk into two regions by inserting an imaginary codimension-1 zero tension brane with transparent boundary condition. To obtain a $2d$ description of the region between the EOW brane and the zero tension brane, one can perform a partial Randall-Sundrum reduction along the σ direction which leads to a gravity theory coupled with the $T\bar{T}$ deformed CFT_2 matter on the EOW brane. The rest of the bulk may be dualized by using the duality discussed in section 2.3. Eventually we have an effective theory including a gravity theory coupled with $T\bar{T}$ deformed CFT matter on EOW brane, and also a $T\bar{T}$ deformed CFT bath glued to EOW brane.

In the effective theory one may utilize the island formula [1, 3] to compute the EE for an interval in the bath. In the boundary description, for a subsystem $A \equiv [0, L]$ in the bath region an island region $I_A = [-a, 0]$ appears in the gravitational sector on the EOW brane. The $2d$ area term in the island formula may be obtained as a part of the $3d$ RT surface area. This is given by the length of the minimal surface (RT surface) that connects zero tension brane to the EOW brane at point $y = a$. The EE of the quantum matter presented in the region $[-a, L]$ may be computed by using the two-point twist

field correlator $\langle \sigma_{g_A^{-1}}(a) \sigma_{g_A}(L) \rangle$. Utilizing these two, the generalized EE in the effective description may be written as [81]

$$S_{\text{gen}}(a) = S_{\text{area}}(a) + S_{\text{matter}}(-a, L),$$

$$= \frac{c}{6} \cosh^{-1} \left[\frac{\sqrt{a^2 + 2az_c \operatorname{sech} \frac{\sigma_0}{\ell} + z_c^2}}{(z_c + a \operatorname{sech} \frac{\sigma_0}{\ell})} \right] + \frac{c}{6} \log \left[\frac{(a+L)^2 \ell}{(z_c + a \operatorname{sech} \frac{\sigma_0}{\ell}) \epsilon_y z_c} \right]. \quad (2.19)$$

Now by extremizing the above expression with respect to a which is only possible perturbatively, we get the extremum value of a similar to eq. (2.17). Now by plugging this extremum value into eq. (2.19) and then expanding the expression linearly in z_c we get the expression for the EE of a subsystem A , which is similar to eq. (2.18) upon utilizing the Brown-Henneaux relation[87].

2.5 Reflected entropy

In this subsection we briefly review the reflected entropy and its computation in CFT_2 as described in [36]. Consider a bipartite quantum system $A \cup B$ in a mixed state ρ_{AB} whose canonical purification involves the doubling of its Hilbert space to define a pure state $|\sqrt{\rho_{AB}}\rangle_{ABA^*B^*}$. The reflected entropy $S_R(A : B)$ is then defined as the von Neumann entropy of the reduced density matrix ρ_{AA^*} as follows

$$S_R(A : B) = S_{vN}(\rho_{AA^*})_{\sqrt{\rho_{AB}}} , \quad (2.20)$$

where ρ_{AA^*} may be obtained by tracing out the degree of freedom of B and B^* from the density matrix $|\sqrt{\rho_{AB}}\rangle \langle \sqrt{\rho_{AB}}|$. The authors in [36] developed a novel replica technique to compute the reflected entropy between two disjoint subsystems $A \equiv [z_1, z_2]$ and $B \equiv [z_3, z_4]$ in a CFT_2 . The reflected entropy may then be obtained in terms of a four-point twist field correlator as follows

$$S_R(A : B) = \lim_{n, m \rightarrow 1} S_n(AA^*)_{\psi_m} = \lim_{n, m \rightarrow 1} \frac{1}{1-n} \log \frac{\left\langle \sigma_{g_A}(z_1) \sigma_{g_A^{-1}}(z_2) \sigma_{g_B}(z_3) \sigma_{g_B^{-1}}(z_4) \right\rangle_{\text{CFT}^{\otimes mn}}}{\left\langle \sigma_{g_m}(z_1) \sigma_{g_m^{-1}}(z_2) \sigma_{g_m}(z_3) \sigma_{g_m^{-1}}(z_4) \right\rangle_{\text{CFT}^{\otimes m}}^n}, \quad (2.21)$$

where m, n are the replica indices⁶ and twist operators σ_{g_A} and σ_{g_B} are inserted at the end points of the subsystems. The conformal dimensions of the operators $\sigma_{g_A}, \sigma_{g_B}$ and σ_{g_m} are given as [36]

$$h \equiv h_A = h_B = \frac{nc}{24} \left(m - \frac{1}{m} \right), \quad h_m = \frac{c}{24} \left(m - \frac{1}{m} \right), \quad h_{AB} = \frac{2c}{24} \left(n - \frac{1}{n} \right). \quad (2.22)$$

It was proved in [36] that the reflected entropy for a bipartite state in a CFT_d in the large central charge limit is dual to twice the minimal EWCS for the bulk static AdS_{d+1} geometry. In the next subsection we review the island and DES formula for the reflected entropy.

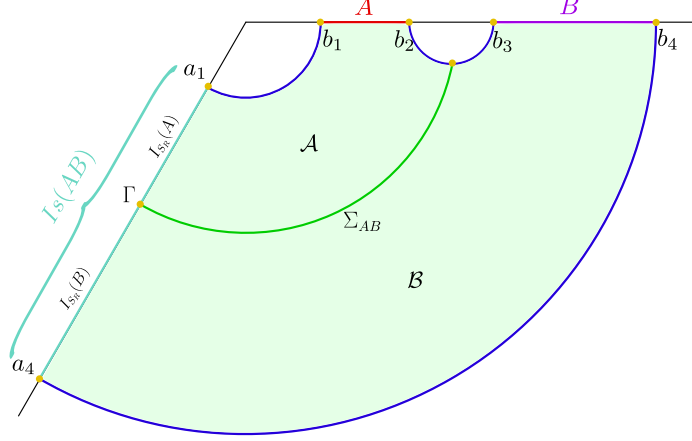


Figure 2: Schematics of the island and DES formula for the reflected entropy. The entanglement wedge of $A \cup B$ is the green shaded region and green curve is the EWCS that splits the bulk into \mathcal{A} and \mathcal{B} . The intersection of the EWCS and EOW brane is denoted by Γ . Figure modify from [33].

2.6 Island and DES formula for Reflected entropy

As described in [43, 44], the island formula for the reflected entropy between two subsystems A and B in asymptotic boundary is given as

$$S_R^{bdy}(A : B) = \min \text{Ext}_{\Gamma} \left\{ S_R^{\text{eff}}(A \cup I_{S_R}(A) : B \cup I_{S_R}(B)) + \frac{\text{Area}[\Gamma]}{2G_N} \right\}, \quad (2.23)$$

where the reflected entropy island $I_{S_R}(A)$ and $I_{S_R}(B)$ divide the entanglement island $I_S(AB)$ into two parts and Γ is the island cross section of $I_{S_R}(A) \cap I_{S_R}(B)$, as shown in fig. 2.

In the bulk description, the reflected entropy may be computed by defect extremal cross section formula as [33]

$$S_R^{bulk}(\mathcal{A} : \mathcal{B}) = \min \text{Ext}_{\Sigma} \left\{ S_R^{\text{eff}}(\mathcal{A} : \mathcal{B}) + \frac{\text{Area}[\Sigma_{AB}]}{2G_N} \right\}. \quad (2.24)$$

where the EWCS (Σ_{AB}) splits the entanglement wedge of $A \cup B$ into two parts \mathcal{A} and \mathcal{B} in the bulk, as depicted in fig. 2. In the above expression, since the conformal matter is only located on the EOW brane, the first term is equal to the reflected entropy between I_A and I_B on the brane and the second term is the area of the EWCS.

3 Zero Temperature

In this section, we analyse the reflected entropy for various bipartite mixed state configurations defined on a fixed time slice of the $T\bar{T}$ deformed $\text{AdS}_3/\text{BCFT}_2$ setup described in section 2.3. We describe the computation of the reflected entropy from both the island and DES perspectives and verify the consistence matching between them.

⁶As discussed in [37, 88, 89], the two replica limits $n \rightarrow 1$ and $m \rightarrow 1$ are non-commuting. In this article, we compute the reflected entropy by first taking $n \rightarrow 1$ and subsequently $m \rightarrow 1$ as suggested in [37, 88].

3.1 Disjoint Subsystems

In this subsection we investigate the reflected entropy corresponding to two disjoint subsystems $A \equiv (b_1, b_2)$ and $B \equiv (b_3, b_4)$ in a fixed time slice of the $T\bar{T}$ deformed $\text{AdS}_3/\text{BCFT}_2$ setup described in section 2. To obtain the various phases of the reflected entropy or the bulk EWCS, first it is required to determine the EE phases for two disjoint subsystems under consideration. Note that, depending on the subsystem size and its location we have two possible phases of the EE. In the following, we describe the computation of the reflected entropy from boundary and bulk perspective for these EE phases and show exact agreement between these two results.

3.1.1 Entanglement Entropy phase-1

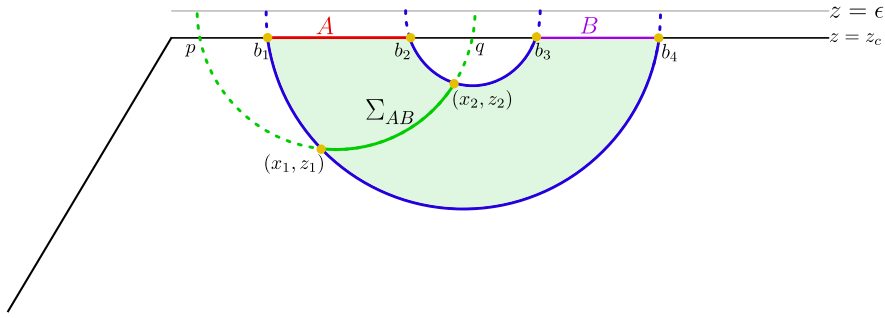


Figure 3: Schematic diagram of the EE phase 1 when the RT surfaces for $A \cup B$ and the EWCS are shown as solid blue and green curve respectively.

In this EE phase we consider that both the subsystems are small and close to each other away from the boundary. Hence the EE is sum of the lengths of two dome-type RT surfaces depicted as solid blue curve in fig. 3. It is well known that the geodesic length between two points (x_1, t_1, z_1) and (x_2, t_2, z_2) on the Poincaré half plane is given as

$$L = \cosh^{-1} \left[\frac{1}{2z_1 z_2} \left((x_2 - x_1)^2 - (t_2 - t_1)^2 + z_1^2 + z_2^2 \right) \right]. \quad (3.1)$$

Now by using the end-points of the subsystem in eq. (3.1), the EE for this configuration may be obtained as

$$S_1 = \frac{1}{2G_N} \log \left[\frac{b_3 - b_2}{z_c} \right] + \frac{1}{2G_N} \log \left[\frac{b_4 - b_1}{z_c} \right]. \quad (3.2)$$

For this EE phase, there is only one phase of the reflected entropy or the bulk EWCS as shown as green curve in fig. 3. In the boundary description, the reflected entropy may be computed by utilizing the following four-point twist field correlator

$$S_R^{\text{bdy}}(A : B) = \lim_{m, n \rightarrow 1} \frac{1}{1 - n} \log \frac{\langle \sigma_{g_A}(b_1) \sigma_{g_A^{-1}}(b_2) \sigma_{g_B}(b_3) \sigma_{g_B^{-1}}(b_4) \rangle}{\langle \sigma_{g_m}(b_1) \sigma_{g_m^{-1}}(b_2) \sigma_{g_m}(b_3) \sigma_{g_m^{-1}}(b_4) \rangle^n}. \quad (3.3)$$

Now by utilizing the form of the four-point function in the large central charge limit [36, 90], we may obtain the reflected entropy as follows

$$S_R^{\text{bdy}}(A : B) = \frac{c}{3} \log \left[\frac{1 + \sqrt{X}}{1 - \sqrt{X}} \right], \quad (3.4)$$

where X is the cross ratio defined as

$$X = \frac{(b_2 - b_1)(b_4 - b_3)}{(b_3 - b_1)(b_4 - b_2)}. \quad (3.5)$$

In the bulk perspective, the EWCS for this phase is proportional to the length of the green geodesic Σ_{AB} as shown in fig. 3. Recall that, on a constant time slice, the RT surfaces/geodesics in the bulk geometry dual to a $T\bar{T}$ deformed CFT_2 are semi-circles centered at the original asymptotic boundary $z = \epsilon$ where the undeformed theory would live. Now utilizing the fact that the minimal curve Σ_{AB}^{min} is perpendicular to both RT surfaces at their intersection points (x_1, z_1) and (x_2, z_2) leads to the following constraint equations

$$\begin{aligned} \left(x_1 - \frac{b_1 + b_4}{2}\right)^2 + z_1^2 &= \left(\frac{b_4 - b_1}{2}\right)^2 + z_c^2, & \left(x_1 - \frac{p + q}{2}\right)^2 + z_1^2 &= \left(\frac{q - p}{2}\right)^2 + z_c^2, \\ \left(x_2 - \frac{b_2 + b_3}{2}\right)^2 + z_2^2 &= \left(\frac{b_3 - b_2}{2}\right)^2 + z_c^2, & \left(x_2 - \frac{p + q}{2}\right)^2 + z_2^2 &= \left(\frac{q - p}{2}\right)^2 + z_c^2, \\ z_1^2 &= -\left(x_1 - \frac{b_1 + b_4}{2}\right)\left(x_1 - \frac{p + q}{2}\right), & z_2^2 &= -\left(x_2 - \frac{b_2 + b_3}{2}\right)\left(x_2 - \frac{p + q}{2}\right), \end{aligned} \quad (3.6)$$

where, the extension of Σ_{AB}^{min} intersects the boundary at the points (p, z_c) and (q, z_c) . The above equations may be solved to fix the endpoints of the curve Σ_{AB}^{min} as

$$\begin{aligned} x_1 &= \frac{b_1^2 b_4 + b_1(-2b_4(b_2 + b_3) + b_2 b_3 + b_4^2 - 2z_c^2) + 2z_c^2(b_2 + b_3 - b_4) + b_2 b_3 b_4}{b_1^2 - b_1(b_2 + b_3) - b_4(b_2 + b_3) + 2b_2 b_3 + b_4^2}, \\ x_2 &= \frac{b_1(b_4(b_2 + b_3) - 2b_2 b_3 + 2z_c^2) - 2z_c^2(b_2 + b_3 - b_4) + b_2 b_3(b_2 + b_3 - 2b_4)}{-b_1(b_2 + b_3 - 2b_4) + b_2^2 - b_4(b_2 + b_3) + b_3^2}, \\ z_1 &= \frac{\sqrt{(b_1 - b_4)^2 + 4z_c^2} \sqrt{(b_1 - b_2)(b_1 - b_3)(b_2 - b_4)(b_3 - b_4) - z_c^2(b_1 - b_2 - b_3 + b_4)^2}}{b_1^2 - b_1(b_2 + b_3) - b_2(b_4 - 2b_3) - b_4(b_3 - b_4)}, \\ z_2 &= \frac{\sqrt{(b_2 - b_3)^2 + 4z_c^2} \sqrt{(b_1 - b_2)(b_1 - b_3)(b_2 - b_4)(b_3 - b_4) - z_c^2(b_1 - b_2 - b_3 + b_4)^2}}{b_2^2 - b_1(b_2 + b_3 - 2b_4) - b_2 b_4 - b_3(b_4 - b_3)}. \end{aligned} \quad (3.7)$$

Now substituting the above values in eq. (3.1) and then linearly expanding the expression in z_c , the bulk EWCS in this phase may be obtained as

$$S_R^{\text{bulk}(A:B)} = \frac{1}{4G_N} \cosh^{-1} \left[\frac{b_1(2b_4 - b_3 - b_2) + b_2(b_4 - 2b_3) - b_3 b_4}{(b_4 - b_1)(b_3 - b_2)} \right]. \quad (3.8)$$

Note that the above expression of the bulk EWCS is precisely equal to half of the reflected entropy computed in eq. (3.4) upon utilizing the Brown-Henneaux relation.

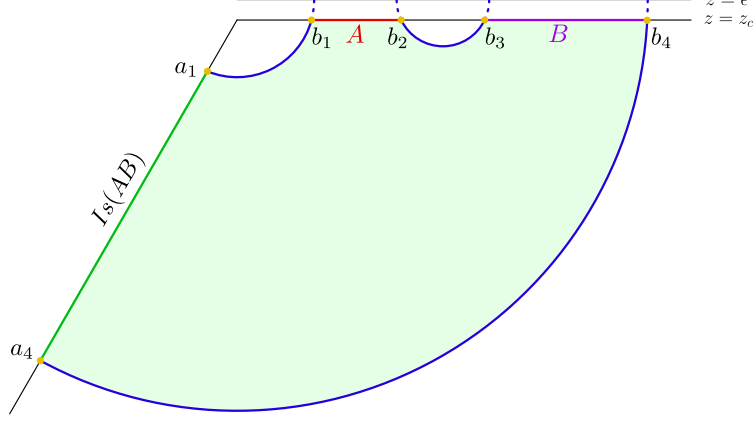


Figure 4: Schematic depicting the EE phase 2 when the RT surface for $A \cup B$ is shown by the solid blue curves.

3.1.2 Entanglement Entropy phase 2

In this EE phase we assume that the subsystem A and B both are close to the boundary, so the EE corresponds to the sum of the lengths of two island surfaces and a dome-type RT surface, shown as blue curves in fig. 4. So the EE for this phase is given as

$$S_2 = \frac{1}{2G_N} \frac{\sigma_0}{\ell} + \frac{1}{2G_N} \log \left[\frac{2\ell \cosh \frac{\sigma_0}{\ell}}{\epsilon_y} \right] + \frac{1}{2G_N} \log \left[\frac{b_3 - b_2}{z_c} \right] + \frac{1}{4G_N} \log \left[\frac{4b_1 b_4}{z_c^2} \right] - \frac{e^{\frac{\sigma_0}{\ell}}}{4G_N} \left(\frac{1}{b_1} + \frac{1}{b_4} \right) z_c, \quad (3.9)$$

where ϵ_y is the finite cutoff for the $T\bar{T}$ deformed CFT on the brane. In this EE phase we observe three distinct phases for the reflected entropy or the bulk EWCS. The computation of the reflected entropy for each phases from the boundary and bulk perspective is described in the following subsection.

Phase-I

The boundary perspective: For this phase, consider that the subsystem A is smaller than the subsystem B , hence the EWCS lands on the island surface corresponding to subsystem A . As there is no island cross section for this phase, the reflected entropy in the boundary description reduces to $S_R^{(\text{eff})}(A : B \cup I_{S_R}(B))$ which may be computed as follows

$$S_R^{(\text{bdy})}(A : B) = S_R^{(\text{eff})}(A : B \cup I_{S_R}(B)) = \lim_{m, n \rightarrow 1} \frac{1}{1-n} \log \frac{\langle \sigma_{g_B^{-1}}(a_1) \sigma_{g_A}(b_1) \sigma_{g_A^{-1}}(b_2) \sigma_{g_B}(b_3) \rangle_{mn}}{\langle \sigma_{g_m^{-1}}(a_1) \sigma_{g_m}(b_1) \sigma_{g_m^{-1}}(b_2) \sigma_{g_m}(b_3) \rangle_m^n}. \quad (3.10)$$

Here a_1 is the intersection point between the island surface corresponding to subsystem A and the EOW brane. As described in [81], the intersection point a_1 may be determined through the extremization of the EE of $A \cup B$ which is given as $a_1 = b_1 - 2z_c e^{\frac{\sigma_0}{\ell}} + \mathcal{O}(z_c^2)$. Utilizing this coordinate value of a_1 and the form of the four-point twist field correlator in the large central charge limit [36, 90] and then expanding the expression linearly in z_c , we

may obtain the reflected entropy as follows

$$S_R^{\text{bdy}}(A : B) = \frac{c}{3} \left(\cosh^{-1} \left[\frac{b_2 b_3 - b_1^2}{b_1 (b_3 - b_2)} \right] + \frac{e^{\frac{\sigma_0}{\ell}} z_c}{b_1} \sqrt{\frac{(b_2 - b_1)(b_3 - b_1)}{(b_1 + b_2)(b_1 + b_3)}} \right) + \mathcal{O}(z_c^2). \quad (3.11)$$

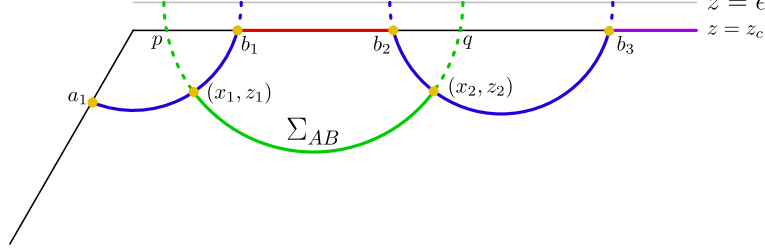


Figure 5: Schematic illustrating the bulk EWCS phase (represented by the solid green curve).

The Bulk perspective: In the bulk description, the curve Σ_{AB} lands on the extremal surface joining b_1 and a_1 and correspondingly the contribution due to the brane matter vanishes identically as the entire island belongs to subsystem B :

$$S_R^{(\text{eff})}(\emptyset : I_B) = 0$$

Hence, the reflected entropy between the bulk regions \mathcal{A} and \mathcal{B} is determined solely by the (minimal) length of the curve Σ_{AB} , depicted as solid green curve in fig. 5.

To compute the length of the curve, we consider the setup in fig. 5. As discussed in the previous phase, the RT surfaces/geodesics are semi-circles in the bulk geometry centered at $z = \epsilon$. Using this fact the geodesic semi-circle joining the boundary points (b_2, z_c) and (b_3, z_c) is given by

$$\left(x - \frac{b_2 + b_3}{2} \right)^2 + z^2 = \left(\frac{b_3 - b_2}{2} \right)^2 + z_c^2 \quad (3.12)$$

In a similar fashion, the radius and centre of the geodesic emanating from (b_1, z_c) and landing on the EOW brane at the location a_1 may be obtained by solving the following equations:

$$(b_1 - x_0)^2 = r^2 \quad , \quad \left(a_1 \tanh \left(\frac{\sigma_0}{\ell} \right) + x_0 \right)^2 + \left(z_c + a_1 \text{sech} \left(\frac{\sigma_0}{\ell} \right) \right)^2 = r^2 \quad (3.13)$$

resulting in

$$x_0 = \frac{b_1^2 - a_1^2 - 2a_1 z_c \text{sech} \left(\frac{\sigma_0}{\ell} \right)}{2 \left(b_1 + a_1 \tanh \left(\frac{\sigma_0}{\ell} \right) \right)} \quad (3.14)$$

$$r = \frac{\sqrt{b_1^2 + a_1^2 + 2a_1 b_1 \tanh \left(\frac{\sigma_0}{\ell} \right)} \sqrt{b_1^2 + a_1^2 + 2a_1 b_1 \tanh \left(\frac{\sigma_0}{\ell} \right) + 4a_1 z_c \text{sech} \left(\frac{\sigma_0}{\ell} \right) + 4z_c^2}}{2 \left(b_1 + a_1 \tanh \left(\frac{\sigma_0}{\ell} \right) \right)} \quad (3.15)$$

Next, we utilize the fact that the minimal curve Σ_{AB}^{\min} is perpendicular to both these circles at their intersection points (x_1, z_1) and (x_2, z_2) as in fig. 5. These geometrical considerations lead to the following constraint equations:

$$\begin{aligned} (x_1 - x_0)^2 + z_1^2 &= r^2, \quad \left(x_1 - \frac{p+q}{2}\right)^2 + z_1^2 = \left(\frac{q-p}{2}\right)^2 + z_c^2, \quad z_1^2 = -(x_1 - x_0) \left(x_1 - \frac{p+q}{2}\right), \\ \left(x_2 - \frac{b_2+b_3}{2}\right)^2 + z_2^2 &= \left(\frac{b_3-b_2}{2}\right)^2 + z_c^2, \quad \left(x_2 - \frac{p+q}{2}\right)^2 + z_2^2 = \left(\frac{q-p}{2}\right)^2 + z_c^2, \\ z_2^2 &= -\left(x_2 - \frac{b_2+b_3}{2}\right) \left(x_2 - \frac{p+q}{2}\right), \end{aligned} \quad (3.16)$$

where, the extension of Σ_{AB}^{\min} intersects the boundary at the points (p, z_c) and (q, z_c) . The above equations may be solved to fix the endpoints of the curve Σ_{AB}^{\min} as follows

$$\begin{aligned} x_1 &= x_0 + \frac{r^2(b_2 + b_3 - 2x_0)}{r^2 + (b_2 - x_0)(b_3 - x_0) - z_c^2}, \quad x_2 = x_0 + \frac{(b_2 + b_3 - 2x_0)((b_2 - x_0)(b_3 - x_0) - r^2 - z_c^2)}{b_2^2 + b_3^2 - 2x_0(b_2 + b_3) - 2r^2 + 2x_0^2 + 2z_c^2}, \\ z_1 &= \frac{r\sqrt{(r^2 - (b_2 - x_0)^2)(r^2 - (b_3 - x_0)^2) - 2z_c^2((x_0 - b_2)(x_0 - b_3) + r^2) + z_c^4}}{(x_0 - b_2)(x_0 - b_3) + r^2 - z_c^2}, \\ z_2 &= \frac{\sqrt{(b_2 - b_3)^2 + 4z_c^2}\sqrt{(r^2 - (b_2 - x_0)^2)(r^2 - (b_3 - x_0)^2) - 2z_c^2((x_0 - b_2)(x_0 - b_3) + r^2) + z_c^4}}{b_2^2 + b_3^2 - 2x_0(b_2 + b_3) - 2r^2 + 2x_0^2 + 2z_c^2}. \end{aligned} \quad (3.17)$$

The length of the minimal surface may now be readily computed and the reflected entropy between the disjoint subsystems is given as follows

$$\begin{aligned} S_R^{\text{bulk}}(\mathcal{A} : \mathcal{B}) &= \frac{1}{2G_N} \cosh^{-1} \left[\frac{(x_2 - x_1)^2 + z_1^2 + z_2^2}{2z_1 z_2} \right] \\ &= \frac{1}{4G_N} \cosh^{-1} \left[\frac{r^2 - (b_2 - x_0)(b_3 - x_0) + z_c^2}{r\sqrt{(b_3 - b_2)^2 + 4z_c^2}} \right] \end{aligned} \quad (3.18)$$

Note that with $a_1 = a_1(z_c)$ determined through the extremization of the entanglement entropy of $A \cup B$, the above expression is non-perturbative in z_c . However, as the extremal solution to a_1 is only determined perturbatively as $a_1 = b_1 - 2e^{\frac{\sigma_0}{\ell}} z_c + \mathcal{O}(z_c^2)$, we expand eq. (3.18) in z_c to obtain

$$S_R^{\text{bulk}}(\mathcal{A} : \mathcal{B}) = \frac{1}{2G_N} \cosh^{-1} \left[\frac{b_2 b_3 - b_1^2}{b_1(b_3 - b_2)} \right] + \frac{e^{\frac{\sigma_0}{\ell}} z_c}{2G_N b_1} \sqrt{\frac{(b_2 - b_1)(b_3 - b_1)}{(b_2 + b_1)(b_3 + b_1)}} + \mathcal{O}(z_c^2). \quad (3.19)$$

Note that when the Brown-Henneaux relation is used, the calculation of the reflected entropy from both the perspective matches exactly.

Phase-II

The boundary perspective: In this phase we assume that the subsystem A is large enough, so the bulk EWCS lands on the EOW brane and divide the EE island into two parts.

In the boundary description, the first term of eq. (2.23) may be obtained by computing the three-point twist field correlator $\langle \sigma_{g_A^{-1}}(b_2) \sigma_{g_B}(b_3) \sigma_{g_B g_A^{-1}}(a) \rangle$ as

$$S_R^{\text{eff}}(A \cup I_{S_R}(A) : B \cup I_{S_R}(B)) = \frac{c}{3} \log \left[\frac{4\ell(a+b_2)(a+b_3)}{\epsilon_y(b_3-b_2)(z_c + a \operatorname{sech} \frac{\sigma_0}{\ell})} \right], \quad (3.20)$$

where ϵ_y is the finite cut-off for the $T\bar{T}$ deformed CFT on the brane and a is the location of the island cross section on the brane. The second term of eq. (2.23) which is the area of the island cross section may be written as follows [81]

$$\text{Area}[\Gamma] = \cosh^{-1} \left[\frac{\sqrt{a^2 + 2az_c \operatorname{sech} \frac{\sigma_0}{\ell} + z_c^2}}{(z_c + a \operatorname{sech} \frac{\sigma_0}{\ell})} \right]. \quad (3.21)$$

By adding these two equations, the reflected entropy in the boundary description for this phase is given as

$$S_R^{\text{bdy}}(A : B) = \frac{c}{3} \log \left[\frac{4\ell(a+b_2)(a+b_3)}{\epsilon_y(b_3-b_2)(z_c + a \operatorname{sech} \frac{\sigma_0}{\ell})} \right] + \frac{c}{3} \cosh^{-1} \left[\frac{\sqrt{a^2 + 2az_c \operatorname{sech} \frac{\sigma_0}{\ell} + z_c^2}}{z_c + a \operatorname{sech} \frac{\sigma_0}{\ell}} \right]. \quad (3.22)$$

The location of the island cross section on the brane may be obtained by extremizing the above expression over a which can only be determined perturbatively as

$$a = \sqrt{b_2 b_3} - \frac{(\sqrt{b_2} + \sqrt{b_3})^2}{2\sqrt{b_2 b_3}} e^{\frac{\sigma_0}{\ell}} z_c + \mathcal{O}(z_c^2). \quad (3.23)$$

Finally substituting the extremum value of a in eq. (3.22) and then linearly expanding the expression in z_c , the reflected entropy for this phase in the boundary description may be obtained as

$$S_R^{\text{bdy}}(A : B) = \frac{c}{3} \left(\frac{\sigma_0}{\ell} + \log \left[\frac{\sqrt{b_3} + \sqrt{b_2}}{\sqrt{b_3} - \sqrt{b_2}} \right] + \log \left[\frac{4\ell \operatorname{sech} \frac{\sigma_0}{\ell}}{\epsilon_y} \right] - \frac{e^{\frac{\sigma_0}{\ell}}}{\sqrt{b_2 b_3}} z_c \right) + \mathcal{O}(z_c^2). \quad (3.24)$$

The bulk perspective: In the bulk description, the curve Σ_{AB} joins dome-type RT surface to the EOW brane at an arbitrary point a and therefore splits the EE island into two parts as shown in fig. 6. Now the first term of eq. (2.24) reduces to $S_R^{\text{eff}}(I_A : I_B)$, which may be computed as

$$S_R^{\text{eff}}(\mathcal{A} : \mathcal{B}) = S_R^{\text{eff}}(I_A : I_B) = \lim_{m,n \rightarrow 1} \frac{1}{1-n} \log \frac{\Pi_i \Omega_i^{2h_i} \langle \sigma_{g_A}(a_1) \sigma_{g_B g_A^{-1}}(a) \sigma_{g_B^{-1}}(a_4) \rangle_{\text{BCFT}^{\otimes mn}}}{\Omega(a_1)^{2nh_{mn}} \Omega(a_4)^{2nh_{mn}} \langle \sigma_{g_m}(a_1) \sigma_{g_m^{-1}}(a_4) \rangle_{\text{BCFT}^{\otimes m}}^n}, \quad (3.25)$$

The BCFT correlator in eq. (3.25) may be expanded in two possible channels: the boundary operator expansion (BOE) and OPE. As explained in [33], the OPE channel in this case never dominates in the large central charge limit. In the BOE channel, the three-point twist field correlator of eq. (3.25) may be factorized to three one-point twist field correlators on the BCFT. Now by utilizing the form of one-point twist field correlator in BCFT and appropriate conformal factors, we may obtain the effective reflected entropy as

$$S_R^{\text{eff}}(I_A : I_B) = \frac{c}{3} \log \frac{2a\ell}{\epsilon_y(z_c + a \operatorname{sech} \frac{\sigma_0}{\ell})}. \quad (3.26)$$

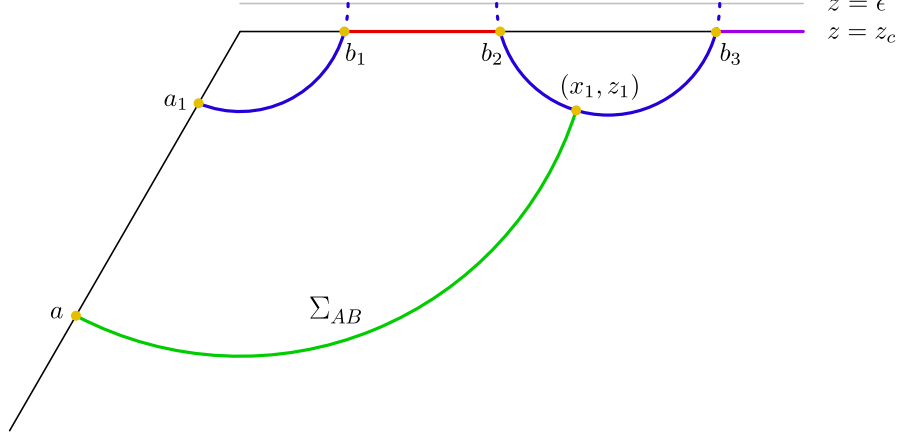


Figure 6: Schematic illustrating the bulk EWCS phase (represented by the solid green curve)

The second term of eq. (2.24) is given by the geodesic length of the curve Σ_{AB} which may be computed by considering the setup depicted in fig. 6. As explained in previous phase, the RT surfaces or geodesics are semi-circles in the bulk geometry centred at $z = \epsilon$. Using this fact the radius and center of the geodesic Σ_{AB} which connects an arbitrary point (x_1, z_1) to $(-a \tanh \frac{\sigma_0}{\ell}, z_c + a \operatorname{sech} \frac{\sigma_0}{\ell})$ on the EOW brane may be obtained by solving the following equations

$$(x_1 - x_c)^2 + z_1^2 = R^2, \quad (-a \tanh \frac{\sigma_0}{\ell} - x_c)^2 + (z_c + a \operatorname{sech} \frac{\sigma_0}{\ell})^2 = R^2, \quad (3.27)$$

which gives

$$x_c = \frac{-a^2 - 2az_c \operatorname{sech} \frac{\sigma_0}{\ell} + x_1^2 + z_1^2 - z_c^2}{2(a \tanh \frac{\sigma_0}{\ell} + x_1)}. \quad (3.28)$$

Utilizing the fact that the curve Σ_{AB} is perpendicular to the dome-type RT surface at their intersection point (x_1, z_1) , we get the following constraints equations

$$\left(x_1 - \frac{b_2 + b_3}{2}\right)^2 + z_1^2 = \left(\frac{b_3 - b_2}{2}\right)^2 + z_c^2, \quad z_1^2 = -\left(x_1 - \frac{b_2 + b_3}{2}\right)(x_1 - x_c). \quad (3.29)$$

Note that the above equation may be solved to determine (x_1, z_1) as follows

$$x_1 = \frac{2b_2b_3 - (b_2 + b_3)x_c - 2z_c^2}{b_2 + b_3 - 2x_c}, \quad z_1 = \sqrt{\frac{((b_2 - x_c)(b_3 - x_c) - z_c^2)((b_3 - b_2)^2 + 4z_c^2)}{(b_2 + b_3 - 2x_c^2)}}. \quad (3.30)$$

Now the second term of eq. (2.24) which is the length of the geodesic between points (x_1, z_1) and $(-a \tanh \frac{\sigma_0}{\ell}, z_c + a \operatorname{sech} \frac{\sigma_0}{\ell})$, may be written as

$$\text{Area}[\Sigma_{AB}] = \cosh^{-1} \left(\frac{(x_1 + a \tanh \frac{\sigma_0}{\ell})^2 + (z_c + a \operatorname{sech} \frac{\sigma_0}{\ell})^2 + z_1^2}{2z_1(z_c + a \operatorname{sech} \frac{\sigma_0}{\ell})} \right). \quad (3.31)$$

The reflected entropy may now be written by adding eq. (3.26) and eq. (3.31) as follows

$$S_R^{\text{bulk}}(\mathcal{A} : \mathcal{B}) = \frac{1}{2G_N} \left[\cosh^{-1} \left(\frac{(x_1 + a \tanh \frac{\sigma_0}{\ell})^2 + (z_c + a \operatorname{sech} \frac{\sigma_0}{\ell})^2 + z_1^2}{2z_1(z_c + a \operatorname{sech} \frac{\sigma_0}{\ell})} \right) + \log \frac{2a\ell}{\epsilon_y(z_c + a \operatorname{sech} \frac{\sigma_0}{\ell})} \right]. \quad (3.32)$$

Now by extremizing the above expression over a perturbatively, we get the extremum value of a as follows

$$a = \sqrt{b_2 b_3} - \frac{(\sqrt{b_2} + \sqrt{b_3})^2}{2\sqrt{b_2 b_3}} e^{\frac{\sigma_0}{\ell}} z_c + \mathcal{O}(z_c^2). \quad (3.33)$$

The reflected entropy for this phase may now be obtained by substituting the extremum value of a in eq. (3.32) and then expanding the expression perturbatively in z_c as

$$S_R^{\text{bulk}}(\mathcal{A} : \mathcal{B}) = \frac{1}{2G_N} \left[\frac{\sigma_0}{\ell} + \log \left[\frac{\sqrt{b_3} + \sqrt{b_2}}{\sqrt{b_3} - \sqrt{b_2}} \right] + \log \left[\frac{4\ell \operatorname{sech} \frac{\sigma_0}{\ell}}{\epsilon_y} \right] - \frac{e^{\frac{\sigma_0}{\ell}}}{\sqrt{b_2 b_3}} z_c \right] + \mathcal{O}(z_c^2). \quad (3.34)$$

Here also the expression of the reflected entropy from the boundary and the bulk perspective matches exactly upon utilizing the Brown-Henneaux relation.

Phase-III

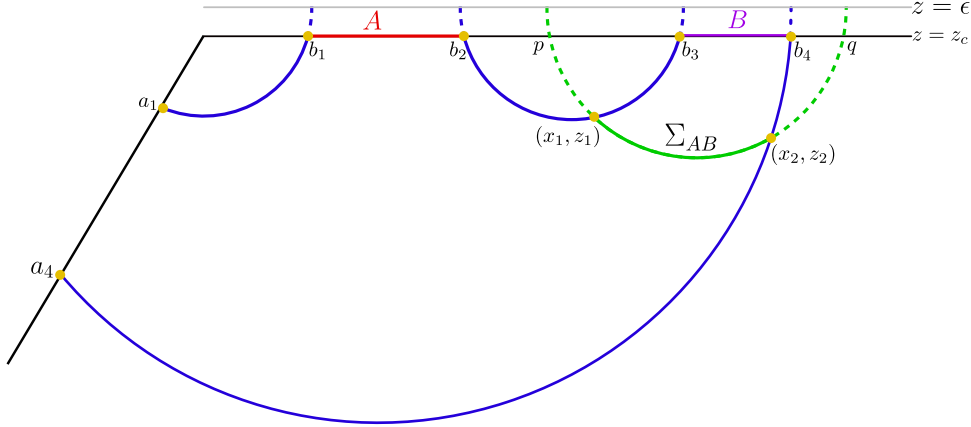


Figure 7: Schematic illustrating the bulk EWCS phase (represented by the solid green curve)

For this phase we assume that the subsystem B is smaller than the subsystem A , hence the EWCS lands on the island surface corresponding to subsystem B shown as the solid green curve in fig. 7. In the boundary description, the reflected entropy may be obtained by exchanging b_1 and b_4 in eq. (3.11) as follows

$$S_R^{\text{bdy}}(A : B) = \frac{c}{3} \left(\cosh^{-1} \left[\frac{b_2 b_3 - b_4^2}{b_4(b_3 - b_2)} \right] + \frac{e^{\frac{\sigma_0}{\ell}} z_c}{b_4} \sqrt{\frac{(b_4 - b_2)(b_4 - b_3)}{(b_4 + b_2)(b_4 + b_3)}} \right) + \mathcal{O}(z_c^2). \quad (3.35)$$

The bulk computation in this case may be done similarly to the [phase-I](#) and the reflected entropy may be computed by interchanging b_1 and b_4 which is exactly matches with eq. (3.35) upon utilizing the Brown-Henneaux relation.

3.2 Adjacent Subsystems

In this subsection we investigate the reflected entropy corresponding to two adjacent subsystems $A \equiv (b_1, b_2)$ and $B \equiv (b_2, b_3)$ in a fixed time slice of the $T\bar{T}$ deformed $\text{AdS}_3/\text{BCFT}_2$ setup described in section 2. Note that for two adjacent subsystems, there are two possible phases of the EE depending on the subsystem size and its location. In the following, we explain the computation of the various reflected entropy phases from both the boundary and bulk perspective.

3.2.1 Entanglement Entropy Phase:1

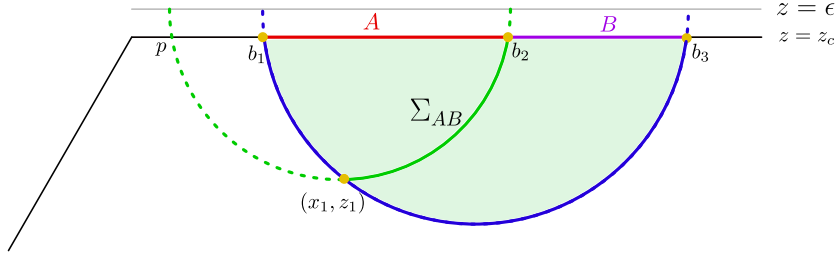


Figure 8: Schematic diagram of the EE phase 1 when the RT surface and the EWCS for $A \cup B$ are shown as blue and green curves.

In this EE phase, we assume that both the subsystems are very small and close to each other away from the boundary. So the EE is proportional to the dome type RT-surface shown as blue curve in fig. 8. Now by utilizing the end points of the subsystems in eq. (3.1), we may obtain the EE for this phase as

$$S_1 = \frac{1}{2G_N} \log \left[\frac{b_3 - b_1}{z_c} \right]. \quad (3.36)$$

In this EE phase, we observe only one phase of the reflected entropy or the bulk EWCS depicted as solid green curve in fig. 8. Now in the boundary description, the reflected entropy reduces to $S_R^{(\text{eff})}(A : B)$ as there is no island cross section on the brane for this phase. Now by utilizing the three-points twist field correlator the reflected entropy may be obtained as

$$S_R^{\text{bdy}}(A : B) = \frac{c}{3} \log \left[\frac{2(b_2 - b_1)(b_3 - b_2)}{z_c(b_3 - b_1)} \right]. \quad (3.37)$$

In the bulk perspective, the EWCS for this phase is proportional to the length of the green geodesic shown in fig. 8. As explained earlier in the bulk geometry the RT surface and geodesic are semi-circles centred at $z = \epsilon$. Utilizing the condition that minimal curve Σ_{AB}^{min} is perpendicular to the RT surface at their intersection point (x_1, z_1) we obtain the following constraint equations

$$\begin{aligned} \left(x_1 - \frac{b_1 + b_3}{2} \right)^2 + z_1^2 &= \left(\frac{b_3 - b_2}{2} \right)^2 + z_c^2, & \left(x_1 - \frac{p + b_2}{2} \right)^2 + z_1^2 &= \left(\frac{b_2 - p}{2} \right)^2 + z_c^2, \\ z_1^2 &= - \left(x_1 - \frac{b_1 + b_3}{2} \right) \left(x_1 - \frac{p + b_2}{2} \right), \end{aligned} \quad (3.38)$$

where the extension of Σ_{AB}^{\min} intersects the boundary at point (p, z_c) . Solving the above equations for (x_1, z_1) leads to

$$\begin{aligned} x_1 &= \frac{b_1^2 b_3 + b_1 (b_2^2 - 4b_2 b_3 + b_3^2) + b_2 (b_2 b_3 + 4z_c^2)}{b_1^2 - 2b_1 b_2 + 2b_2^2 - 2b_2 b_3 + b_3^2 + 4z_c^2}, \\ z_1 &= \frac{\sqrt{(b_1 - b_3)^2 + 4z_c^2} \sqrt{(b_1 - b_2)^2 (b_2 - b_3)^2 + z_c^2 (b_1 - b_3)^2 + 4z_c^4}}{2b_1 b_2 + 2b_2 b_3 - 2b_2^2 - b_1^2 - b_3^2 - 4z_c^2}. \end{aligned} \quad (3.39)$$

Now substituting the above values in eq. (3.1) and then expanding the expression linearly in z_c , we may obtain the bulk EWCS in this phase which is exactly half of the reflected entropy computed in eq. (3.37) upon utilizing the Brown-Henneaux relation.

3.2.2 Entanglement Entropy Phase:2

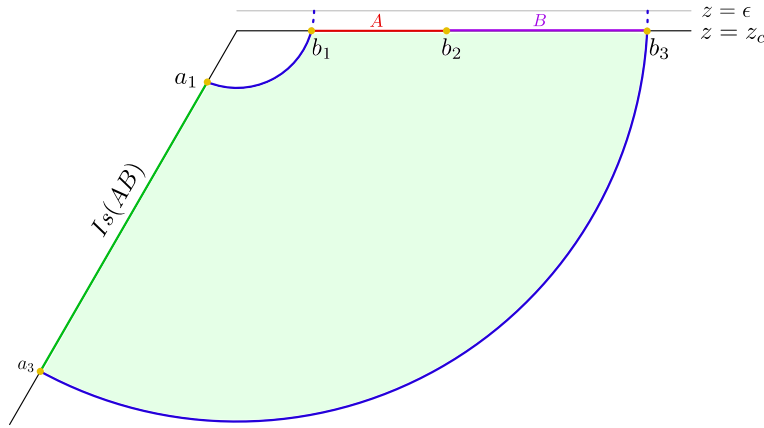


Figure 9: Schematic diagram of the EE phase 2 when the RT surface for $A \cup B$ are shown as blue curve.

In this EE phase we consider that the subsystem A and B are close to the boundary, hence the EE is proportional to the sum of length of two island surfaces, depicted as blue curves in fig. 9. The EE for this configuration is given as

$$S_2 = \frac{1}{2G_N} \frac{\sigma_0}{\ell} + \frac{1}{2G_N} \log \left[\frac{2\ell \cosh \frac{\sigma_0}{\ell}}{\epsilon_y} \right] + \frac{1}{4G_N} \log \left[\frac{4b_1 b_3}{z_c^2} \right] - \frac{e^{\frac{\sigma_0}{\ell}}}{4G_N} \left(\frac{1}{b_1} + \frac{1}{b_3} \right) z_c. \quad (3.40)$$

For this EE phase, there are three possible phases of the reflected entropy or the bulk EWCS, depending on the subsystems size and location. In the following, we explain the computation of the reflected entropy in the boundary and bulk perspective.

Phase-I

The boundary perspective: In this phase we assume that the subsystem A is smaller than the subsystem B , so the EWCS lands on the island surface corresponding to the subsystem A . There is no island cross section for this phase, hence in the boundary description,

the reflected entropy is equal to $S_R^{(\text{eff})}(A : B \cup I_{S_R}(B))$ which may be computed by utilizing the following expression

$$S_R^{\text{bdy}}(A : B) = S_R^{\text{eff}}(A : B \cup I_{S_R}(B)) = \lim_{m,n \rightarrow 1} \frac{1}{1-n} \log \frac{\langle \sigma_{g_A}(b_1) \sigma_{g_B g_A^{-1}}(b_2) \sigma_{g_A^{-1}}(a_1) \rangle}{\langle \sigma_{g_m}(b_1) \sigma_{g_m^{-1}}(a_1) \rangle^n}. \quad (3.41)$$

Here a_1 a point on the EOW brane where island surface of A intersects with the EOW brane. As described in [81] the intersection point may be obtained by extremizing the EE of subsystems $A \cup B$ as $a_1 = b_1 - 2z_c e^{\frac{\sigma_0}{l}}$. Now by utilizing this value in the form of the three-point twist field correlator and then expanding it linearly in z_c , we may obtain the reflected entropy for this phase as follows

$$S_R^{\text{bdy}}(A : B) = \frac{c}{3} \left(\log \left[\frac{(b_2 - b_1)(b_2 + b_1)}{b_1 z_c} \right] + \frac{(b_2 - b_1) e^{\frac{\sigma_0}{l}}}{b_1(b_2 + b_1)} z_c \right). \quad (3.42)$$

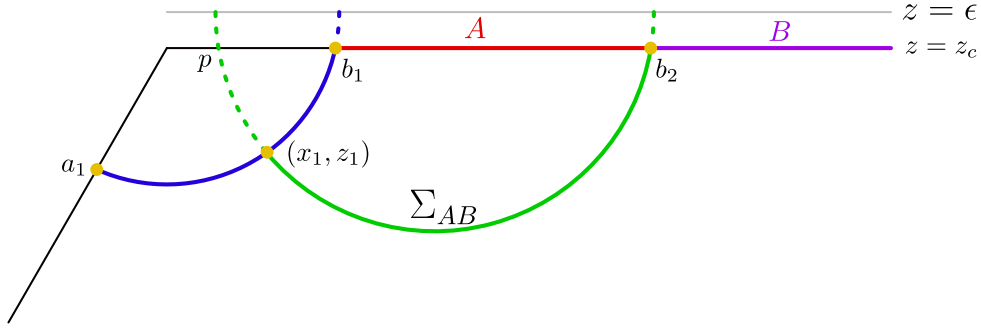


Figure 10: Diagrammatic illustration of the bulk EWCS between subsystems A and B (depicted as solid green curves.)

The bulk perspective: In the bulk description, the curve Σ_{AB} connects point b_2 to a point (x_1, z_1) on the extremal surface joining b_1 and a_1 and hence the first term of eq. (2.24) vanishes as the entire island belongs to the subsystem B . Therefore, the reflected entropy for this case is given by the (minimal) length of the curve Σ_{AB} shown as green curve in fig. 10. As explained earlier in the bulk geometry these RT surfaces or geodesics are semi-circles centred at $z = \epsilon$. The radius and centre of the geodesic connecting b_1 and a_1 is given in eq. (3.14). Now by using the fact that minimal curve Σ_{AB}^{min} is perpendicular to this geodesic or circle at their intersection point (x_1, z_1) , we get the following set of the constraint equations

$$(x_1 - x_0)^2 + z_1^2 = r^2, \quad \left(x_1 - \frac{p + b_2}{2} \right)^2 + z_1^2 = \left(\frac{b_2 - p}{2} \right)^2 + z_c^2, \quad z_1^2 = -(x_1 - x_0) \left(x_1 - \frac{p + b_2}{2} \right), \quad (3.43)$$

where the extension of Σ_{AB}^{min} intersects the boundary at point (p, z_c) . Now by solving the above equations we may obtain the point (x_1, z_1) as follows

$$x_1 = x_0 + \frac{2r^2(b_2 - x_0)}{r^2 + (b_2 - x_0)^2 + z_c^2}, \quad z_1 = \frac{r \sqrt{((b_2 - x_0)^2 - r^2)^2 + 2((b_2 - x_0)^2 + r^2)z_c^2 + z_c^4}}{(b_2 - x_0)^2 + r^2 + z_c^2}, \quad (3.44)$$

where r and x_0 is given in eq. (3.14). Here the length of the minimal surface may be computed directly and therefore the reflected entropy for this phase is given as

$$\begin{aligned} S_R^{\text{bulk}}(\mathcal{A} : \mathcal{B}) &= \frac{1}{2G_N} \cosh^{-1} \left[\frac{(x_1 - b_2)^2 + z_1^2 + z_c^2}{2z_1 z_c} \right] \\ &= \frac{1}{2G_N} \cosh^{-1} \left[\frac{\sqrt{((b_2 - x_0)^2 - r^2)^2 + 2((b_2 - x_0)^2 + r^2)z_c^2 + z_c^4}}{2r z_c} \right] \end{aligned} \quad (3.45)$$

Now substituting the value of x_0 , r and $a_1 = b_1 - 2e^{\frac{\sigma_0}{\ell}} z_c + \mathcal{O}(z_c^2)$ in eq. (3.45) and then expand perturbatively in z_c , we obtain

$$S_R^{\text{bulk}}(\mathcal{A} : \mathcal{B}) = \frac{1}{2G_N} \left(\log \left[\frac{(b_2 - b_1)(b_2 + b_1)}{b_1 z_c} \right] + \frac{(b_2 - b_1) e^{\frac{\sigma_0}{\ell}}}{b_1(b_2 + b_1)} z_c \right) + \mathcal{O}(z_c^2). \quad (3.46)$$

It should be noted that the reflected entropy from both the perspective matches exactly when the Brown-Henneaux relation is used.

Phase-II

In this reflected entropy phase we assume that the subsystem A is large enough, hence the EWCS lands on the EOW brane. For this case there is a non-trivial island cross section on the brane which divides the entanglement island into two parts. In the boundary description, eq. (2.23) may be written as

$$S_R^{\text{bdy}}(A : B) = \frac{c}{3} \log \left[\frac{\ell(a + b_2)^2}{\epsilon_y z_c (z_c + a \text{sech} \frac{\sigma_0}{\ell})} \right] + \frac{c}{3} \cosh^{-1} \left[\frac{\sqrt{a^2 + 2a z_c \text{sech} \frac{\sigma_0}{\ell} + z_c^2}}{z_c + a \text{sech} \frac{\sigma_0}{\ell}} \right], \quad (3.47)$$

where a is the location of the island cross section on the brane. The first term of the above expression may be obtained by utilizing two-point twist field correlator $\langle \sigma_{g_A g_B^{-1}}(b_2) \sigma_{g_B g_A^{-1}}(a) \rangle$ and the second term is the area of island cross section given in eq. (3.21). Note that to obtain the location of the island cross section on the EOW brane, one has to extremize the above expression over a . The extremization procedure can only be done perturbatively in the present scenario. By extremizing eq. (3.47) over a , we get the extremum value of a as

$$a = b_2 - 2z_c e^{\frac{\sigma_0}{\ell}} + \mathcal{O}(z_c^2). \quad (3.48)$$

Substituting eq. (3.48) in eq. (3.47) and then expanding the expression linearly in z_c the reflected entropy in the boundary description may be obtained as

$$S_R^{\text{bdy}}(A : B) = \frac{c}{3} \left[\frac{\sigma_0}{\ell} + \log \left(\frac{4b_2 \ell \cosh \frac{\sigma_0}{\ell}}{z_c \epsilon_y} \right) - \frac{z_c e^{\frac{\sigma_0}{\ell}}}{b_2} \right] + \mathcal{O}(z_c^2). \quad (3.49)$$

The bulk perspective: In the bulk description, the curve Σ_{AB} connects point (b_2, z_c) to a point a on the EOW brane and thus splits the EE island into two parts, as depicted in fig. 11. The first term of eq. (2.24) i.e. the effective reflected entropy is given in

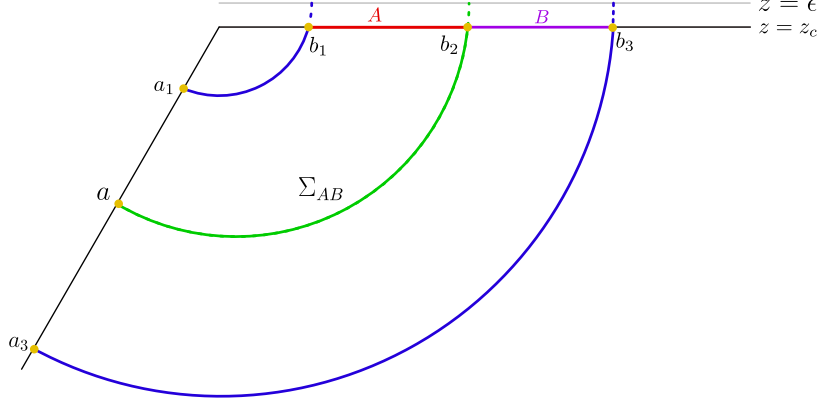


Figure 11: Diagrammatic illustration of the EWCS between subsystems A and B (depicted as the solid green curves.)

eq. (3.26). The second term which is basically the geodesic length between points (b_2, z_c) and $(-a \tanh \frac{\sigma_0}{\ell}, z_c + a \operatorname{sech} \frac{\sigma_0}{\ell})$ is given as follows

$$\text{Area}[\Sigma_{AB}] = \cosh^{-1} \left(\frac{(b_2 + a \tanh \frac{\sigma_0}{\ell})^2 + (z_c + a \operatorname{sech} \frac{\sigma_0}{\ell})^2 + z_c^2}{2z_c(z_c + a \operatorname{sech} \frac{\sigma_0}{\ell})} \right). \quad (3.50)$$

By adding eqs. (3.26) and (3.50), we can write the reflected entropy from the bulk side as

$$S_R^{\text{bulk}}(\mathcal{A} : \mathcal{B}) = \frac{1}{2G_N} \cosh^{-1} \left(\frac{(b_2 + a \tanh \frac{\sigma_0}{\ell})^2 + (z_c + a \operatorname{sech} \frac{\sigma_0}{\ell})^2 + z_c^2}{2z_c(z_c + a \operatorname{sech} \frac{\sigma_0}{\ell})} \right) + \frac{c}{3} \log \frac{2a\ell}{\epsilon_y(z_c + a \operatorname{sech} \frac{\sigma_0}{\ell})}. \quad (3.51)$$

Now by extremizing the above expression over a which is only possible perturbatively, we may get the extremum value of a as follows

$$a = b_2 - 2z_c e^{\frac{\sigma_0}{\ell}} + \mathcal{O}(z_c^2). \quad (3.52)$$

Substituting the value of a in eq. (3.51) and then expanding the expression perturbatively in z_c , the reflected entropy for this phase from the bulk side may be obtained as

$$S_R^{\text{bulk}}(\mathcal{A} : \mathcal{B}) = \frac{1}{2G_N} \left[\frac{\sigma_0}{\ell} + \log \left(\frac{4b_2\ell \cosh \frac{\sigma_0}{\ell}}{z_c \epsilon_y} \right) - \frac{z_c e^{\frac{\sigma_0}{\ell}}}{b_2} \right] + \mathcal{O}(z_c^2). \quad (3.53)$$

Here also the reflected entropy computed from the boundary perspective exactly matches with the bulk perspective upon utilizing the Brown-Henneaux relation.

Phase-III

In this phase we consider that the subsystem B is smaller than the subsystem A , so the bulk EWCS lands on the island surface corresponding to the subsystem B , depicted as solid green curve in fig. 12. Now the reflected entropy in the boundary description may be obtained by interchanging b_1 and b_3 in eq. (3.42) as

$$S_R^{\text{bdy}}(A : B) = \frac{c}{3} \left(\log \left[\frac{(b_3 - b_2)(b_3 + b_2)}{b_3 z_c} \right] + \frac{(b_3 - b_2) e^{\frac{\sigma_0}{\ell}}}{b_3(b_3 + b_2)} z_c \right) + \mathcal{O}(z_c^2). \quad (3.54)$$

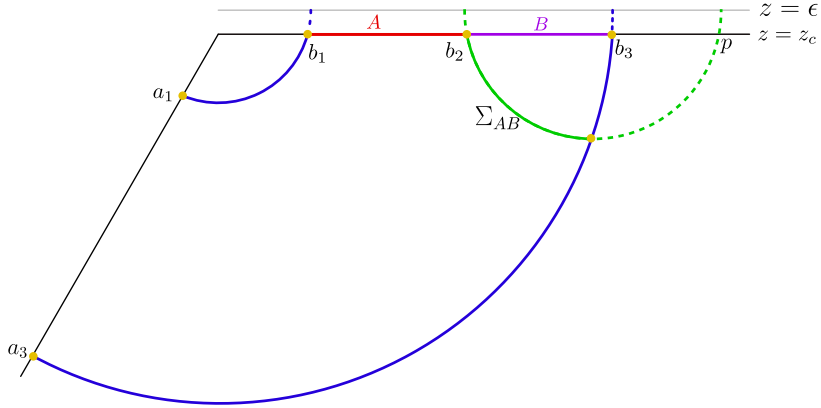


Figure 12: Schematic illustrating the bulk EWCS phase between A and B (represented by the solid green curve.)

In the bulk description, the computation of the reflected entropy may be done similarly to [phase-I](#) and the expression for the reflected entropy may be obtained by exchanging the b_1 and b_3 which exactly matches with eq. (3.54) upon utilizing the Brown-Henneaux relation.

4 Time dependent reflected entropy in black hole evaporation

In this section, we study the reflected entropy between the black hole interiors and radiation region in a time dependent $\text{AdS}_3/\text{BCFT}_2$ scenario with the $T\bar{T}$ deformation involving an eternal black hole in the effective two-dimensional description [81]. We also plot the analogue of the Page curve for the reflected entropy and observe the correction due to $T\bar{T}$ deformation.

4.1 The emergence of a 2d eternal black hole

We begin by reviewing how a 2d eternal black hole emerges from the $\text{AdS}_3/\text{BCFT}_2$ model [16, 32, 33]. As discussed in the previous section, the holographic dual to a 2d BCFT is an AdS_3 geometry with a codimension-1 EOW brane. The metric of Euclidean AdS_3 bulk is given as

$$\begin{aligned} ds^2 &= \frac{\ell^2}{z^2} (d\tau^2 + dz^2 + dx^2) \\ &= d\sigma^2 + \frac{\ell^2 \cosh^2 \frac{\sigma}{\ell}}{y^2} (d\tau^2 + dy^2). \end{aligned} \quad (4.1)$$

We consider the bulk geometry to be bounded by a BCFT defined on a half plane given by $(x, \tau > 0)$ ⁷. The EOW brane is located at $\tau = -z \sinh \frac{\sigma_0}{\ell}$, with σ_0 being a constant.

⁷In Euclidean spacetime, spacelike and timelike coordinates are equivalent, and thus x and τ can be interchanged as per convenience.

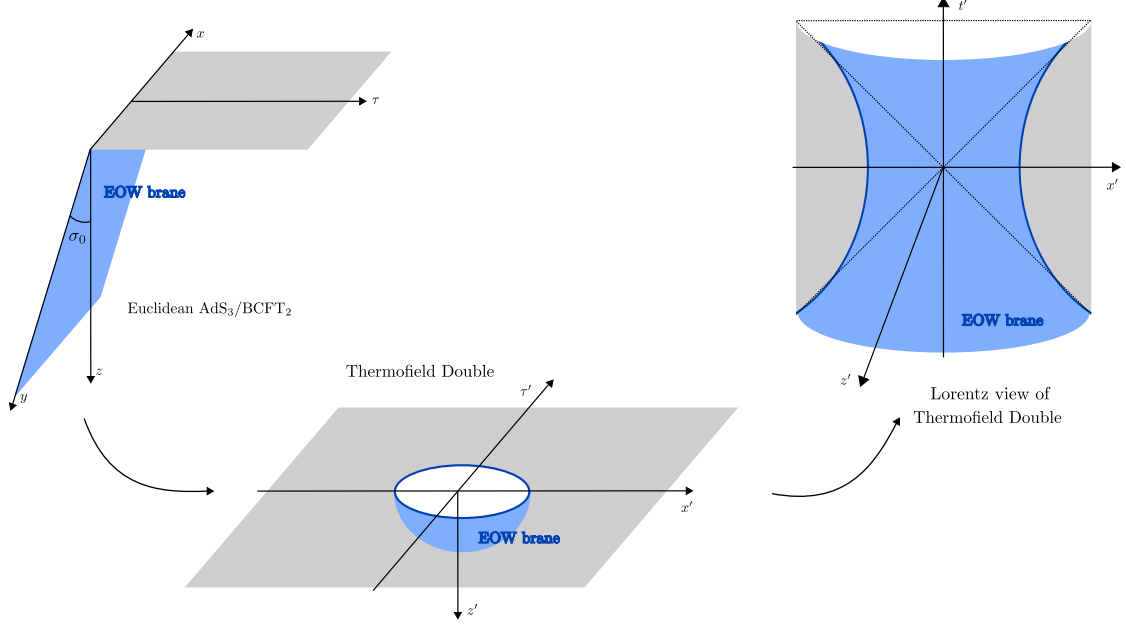


Figure 13: In the first step a global conformal transformation takes us from from Euclidean $\text{AdS}_3/\text{BCFT}_2$ to a thermofield double state. It is followed by analytically continuing $\tau' \rightarrow it'$ which provides us the Lorentz view of the TFD.

Using the set of global conformal transformations as follows

$$\begin{aligned}\tau &= \frac{2(x'^2 + \tau'^2 + z'^2 - 1)}{(\tau' + 1)^2 + x'^2 + z'^2}, \\ x &= \frac{4x'}{(\tau' + 1)^2 + x'^2 + z'^2}, \\ z &= \frac{4z'}{(\tau' + 1)^2 + x'^2 + z'^2},\end{aligned}\tag{4.2}$$

the boundary of the BCFT and the EOW brane may be mapped to a circle and a part of a sphere respectively as

$$x'^2 + \tau'^2 = 1, \quad (z' + \sinh \frac{\sigma_0}{\ell})^2 + x'^2 + \tau'^2 = \cosh^2 \frac{\sigma_0}{\ell}.\tag{4.3}$$

Note that the global conformal transformations given by eq. (4.2) ensure that the metric of the bulk as well as the metric induced on the EOW brane is preserved. The inverse transformations to eq. (4.2) are provided in [34].

From the above bulk configuration, a two-sided 2d eternal black hole may be obtained using the partial Randall-Sundrum reduction and $\text{AdS}_3/\text{BCFT}_2$ correspondence [31]. The black hole appears on the EOW brane, which in the effective 2d description is coupled to the BCFT_2 outside the circle in eq. (4.3). This hybrid manifold may be described as analytical continuation of $\tau' \rightarrow it'$ followed by introduction of the Rindler coordinates (X, T) as [3]

$$x' = e^X \cosh T, \quad t' = e^X \sinh T,\tag{4.4}$$

which capture the near-horizon geometry of the black hole.

$T\bar{T}$ deformation

As elaborated in section 2, the boundary of AdS_3 is pushed into the bulk to a finite radial cut-off surface when the theory is deformed by the $T\bar{T}$ operator. As a result, the EOW brane is shifted to $\tau = -(z - z_c) \sinh \frac{\sigma_0}{\ell}$. The boundary of the BCFT and the brane profile in eq. (4.3) is thus modified as

$$x'^2 + \tau'^2 = 1 - z_c'^2, \quad (z' + \sinh \frac{\sigma_0}{\ell})^2 + x'^2 + \tau'^2 = \cosh^2 \frac{\sigma_0}{\ell} + 2z'_c \sinh \frac{\sigma_0}{\ell}, \quad (4.5)$$

respectively, where the relation between z'_c and z_c is provided by eq. (4.2). Subsequently, we may once again obtain the two-sided 2d eternal black hole via transformations in eq. (4.4), using the partial Randall-Sundrum reduction and $\text{AdS}_3/\text{BCFT}_2$ correspondence. The UV cut-off in the Rindler coordinates z_R can be related to z'_c as

$$z'_c = z_R e^X, \quad (4.6)$$

where z_R is assumed to be a constant everywhere.

4.2 Reflected entropy between black hole interiors

In this section we compute the time dependent reflected entropy between different regions of the black hole interior in presence of $T\bar{T}$ deformation. As illustrated in figs. 14 and 15, the black hole region is defined by the spacelike interval between points $Q \equiv (\tau'_1, -x'_1, z'_1)$ and $P \equiv (\tau'_1, x'_1, z'_1)$ [32, 33]. To simplify the computation we initially work in the unprimed coordinate system. By employing the transformations described in eq. (4.2), the endpoints of the black hole region, given by $(\tau'_1, \pm x'_1, z'_1)$ in the primed coordinates, may be mapped to $(\tau_1, \pm x_1, z_1)$ in the unprimed coordinates.

The configuration of the black hole region—specifically, its size and location determines whether we encounter an island or a no-island phase for the entanglement entropy. Correspondingly, for each EE phase there are various possible reflected entropy phases between the black hole subsystems $B_L = |QO|$ and $B_R = |OP|$ (denoted by the red lines in fig. 14 and related illustrations), O being the extremal point on the brane.

4.2.1 Entanglement Entropy Phase: 1

In this phase, EE does not include any contribution from an island, hence the EE is determined by the length of the Hartman-Maldacena (HM) surface [91] OP , depicted by the green curve in Figure 14. As evaluated in [81], in this phase the EE in Rindler coordinates is given by

$$S(B_L \cup B_R) = \frac{c}{3} \log \frac{2 \cosh T}{z_R}. \quad (4.7)$$

In this scenario, there exists only a single possible phase of the reflected entropy or the bulk EWCS between the black hole regions B_L and B_R shown as solid yellow line in Figure 14. In the following we explain the computation of this both from the boundary and bulk perspectives.

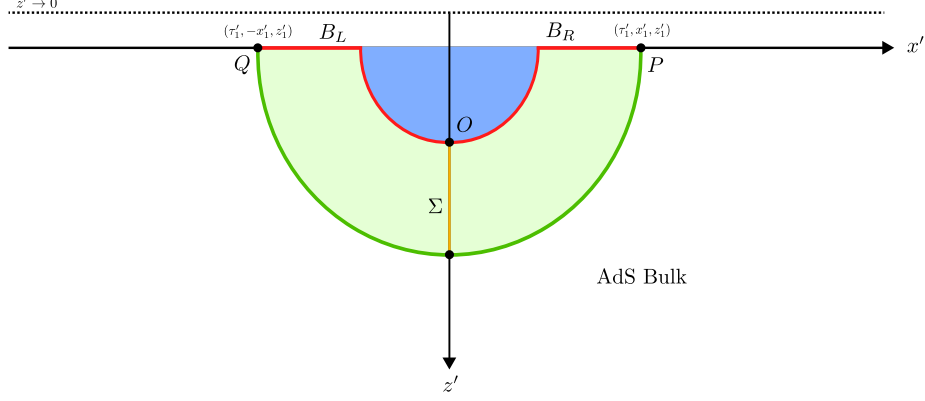


Figure 14: This diagram illustrates the no-island phase of entanglement entropy of the black hole region. The red lines represent the black hole interior, green line represents the HM surface connecting the endpoints of the black hole region, while the yellow line represents the entanglement wedge cross section.

Boundary description

In the boundary description, the reflected entropy between B_L and B_R may be computed using eq. (2.23), where the first term (the effective term) is given by a three-point twist field correlators as

$$S_R^{\text{eff}}(B_L : B_R) = \lim_{m,n \rightarrow 1} \frac{1}{1-n} \log \frac{\Omega_O^{2h_{g_A^{-1}g_B}} \langle \sigma_{g_A}(P) \sigma_{g_A^{-1}g_B}(O) \sigma_{g_B^{-1}}(Q) \rangle_{CFT^{\otimes mn}}}{\langle \sigma_{g_m}(P) \sigma_{g_m}(Q) \rangle_{CFT^{\otimes m}}^n}, \quad (4.8)$$

where Ω_O is the conformal factor. By adding the area term to S_R^{eff} , which has the same functional form as eq. (3.21), the generalised reflected entropy may be written as

$$\begin{aligned} S_R^{\text{bdy}}(B_L : B_R) &= S_R^{\text{eff}}(B_L : B_R) + S_{\text{area}}(O) \\ &= \frac{c}{3} \left(\log \left[\frac{x_1^2 + (\tau_1 + y)^2}{x_1} \right] + \log \frac{\ell}{\epsilon_y(z_1 + y \operatorname{sech} \frac{\sigma_0}{\ell})} \right) \\ &\quad + \frac{c}{3} \cosh^{-1} \left[\frac{\sqrt{y^2 + z_1^2 + 2z_1 y \operatorname{sech} \frac{\sigma_0}{\ell}}}{z_1 + y \operatorname{sech} \frac{\sigma_0}{\ell}} \right], \end{aligned} \quad (4.9)$$

with y being the brane coordinate of O . Now by extremizing the above expression over y perturbatively in z_1 , we get the extremum value of y as

$$y = \sqrt{x_1^2 + \tau_1^2} - z_1 e^{\frac{\sigma_0}{\ell}} \left(\frac{\tau_1 + \sqrt{x_1^2 + \tau_1^2}}{\sqrt{x_1^2 + \tau_1^2}} \right) + \mathcal{O}(z_1^2). \quad (4.10)$$

Putting back y into eq. (4.9) the extremized reflected entropy is obtained upto first order in z_1 as

$$S_R^{\text{bdy}}(B_L : B_R) = \frac{c}{3} \left(\log \left[\frac{\tau_1 + \sqrt{x_1^2 + \tau_1^2}}{x_1} \right] + \log \frac{2\ell}{\epsilon_y \operatorname{sech} \frac{\sigma_0}{\ell}} + \frac{\sigma_0}{\ell} \right) - \frac{c}{3} \frac{z_1 e^{\frac{\sigma_0}{\ell}}}{\sqrt{x_1^2 + \tau_1^2}} + \mathcal{O}(z_1^2). \quad (4.11)$$

Bulk description

In the bulk description, the reflected entropy between B_L and B_R is computed using eq. (2.24). The set up for computing the length of the entanglement wedge cross section Σ (denoted by the yellow line in fig. 14) is described in [33]. As discussed previously, the calculation is initially carried out in the unprimed coordinates for simplicity. Following [33], the computation is reduced to finding the geodesic length between points $(\tau_1, x, \sqrt{-x^2 + x_1^2 + z_1^2})$ (see appendix A.1) and $O \equiv (-y \tanh \frac{\sigma_0}{\ell}, x_y, y \operatorname{sech} \frac{\sigma_0}{\ell} + z_1)$ on the brane, which is given using eq. (3.1) as [11, 12]

$$\text{Area}[\Sigma] = \cosh^{-1} \left[\frac{x_1^2 - 2xx_y + x_y^2 + y^2 + 2z_1^2 + \tau_1^2 + 2yz_1 \operatorname{sech} \frac{\sigma_0}{\ell} + 2y\tau_1 \tanh \frac{\sigma_0}{\ell}}{2\sqrt{-x^2 + x_1^2 + z_1^2}(z_1 + y \operatorname{sech} \frac{\sigma_0}{\ell})} \right]. \quad (4.12)$$

Adding the defect term eq. (3.26) to eq. (4.12), the generalized holographic reflected entropy is given using eq. (2.24) as

$$S_R^{\text{bulk}}(B_L : B_R) = \frac{c}{3} \cosh^{-1} \left[\frac{x_1^2 - 2xx_y + x_y^2 + y^2 + 2z_1^2 + \tau_1^2 + 2yz_1 \operatorname{sech} \frac{\sigma_0}{\ell} + 2y\tau_1 \tanh \frac{\sigma_0}{\ell}}{2\sqrt{-x^2 + x_1^2 + z_1^2}(z_1 + y \operatorname{sech} \frac{\sigma_0}{\ell})} \right] + \frac{c}{3} \log \frac{2y\ell}{\epsilon_y(z_1 + y \operatorname{sech} \frac{\sigma_0}{\ell})}. \quad (4.13)$$

Extremizing the above equation over y and x_y , we get the extremum values as (up to first order in z_1),

$$y = \sqrt{x_1^2 + \tau_1^2} - z_1 \left(\frac{\tau_1 + \sqrt{x_1^2 + \tau_1^2}}{\sqrt{x_1^2 + \tau_1^2}} \right) e^{\frac{\sigma_0}{\ell}} + \mathcal{O}(z_1^2), \quad x_y = x = 0. \quad (4.14)$$

Inserting the value of y and x_y in eq. (4.13), we obtain the reflected entropy in the bulk description which is identical with the field theory computation outlined in eq. (4.11). Applying the transformations detailed in eqs. (4.2), (4.4) and (4.6), the reflected entropy can be expressed in terms of the Rindler coordinates as

$$S_R^{\text{bulk}}(B_L : B_R) = \frac{c}{3} \left(\log \left[\frac{\sinh X_1 + \sqrt{\cosh^2 T + \sinh^2 X_1}}{\cosh T} \right] + \log \frac{2\ell}{\epsilon_y \operatorname{sech} \frac{\sigma_0}{\ell}} + \frac{\sigma_0}{\ell} \right) - \frac{c}{3} \frac{z_R e^{\frac{\sigma_0}{\ell}}}{\sqrt{\cosh^2 T + \sinh^2 X_1}} + \mathcal{O}(z_R^2), \quad (4.15)$$

where X_1 is a fixed constant specifying the boundary of the black hole region for a constant T slice in the Rindler coordinates.

4.2.2 Entanglement Entropy Phase: 2

As depicted in fig. 15, this phase of EE includes contributions from the island regions. Consequently, the EE is determined by the combined lengths of the two island surfaces and two RT surfaces denoted by the green curves expressed as [81]

$$S(B_L \cup B_R) = \frac{c}{3} \left(\frac{\sigma_0}{\ell} + \log \frac{2 \sinh X_1}{z_R} + \log \frac{2\ell}{\epsilon_y \operatorname{sech} \frac{\sigma_0}{\ell}} \right) - \frac{c}{3} \frac{z_R e^{\frac{\sigma_0}{\ell}}}{\sinh X_1}. \quad (4.16)$$

Similar to the previous EE phase, this configuration leads to a single possible reflected entropy phase between black hole subsystems $B_L = |QQ'|$ and $B_R = |PP'|$, where Q' and P' are the points where the disconnected RT surfaces and the brane intersect. The detailed computation of the reflected entropy in this scenario is as follows.

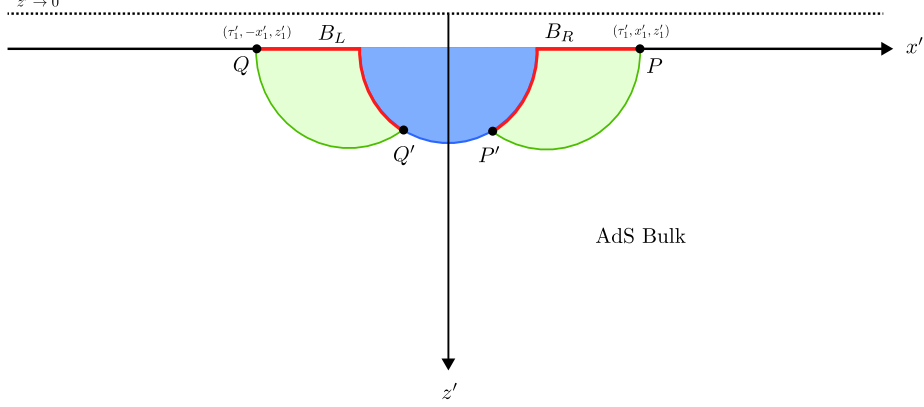


Figure 15: The illustration depicts the island phase of EE of the black hole interior. The green lines represent the disconnected RT surfaces. We have no entanglement wedge cross section in this phase.

Boundary description

In this configuration, there is no contribution from the area term since the two regions B_L and B_R do not intersect. Consequently, the second term in eq. (2.23) no longer contributes in this case. Therefore the generalized reflected entropy is simply the effective reflected entropy term between $|QQ'|$ and $|PP'|$, which can be computed from a four-point correlation function of twist operators at brane points Q' and P' , and boundary points Q and P as

$$S_R^{\text{bdy}} = S_R^{\text{eff}} = \lim_{m,n \rightarrow 1} \frac{1}{1-n} \log \frac{\Omega_{Q'}^{2h_{g_A}} \Omega_{P'}^{2h_{g_A}} \langle \sigma_{g_A}(Q') \sigma_{g_A^{-1}}(Q) \sigma_{g_B}(P') \sigma_{g_B^{-1}}(P) \rangle_{CFT^{\otimes mn}}}{\Omega_{Q'}^{2nh_m} \Omega_{P'}^{2nh_m} \langle \sigma_{g_m}(Q') \sigma_{g_m}(Q) \sigma_{g_m}(P') \sigma_{g_m}(P) \rangle_{CFT^{\otimes m}}^n}. \quad (4.17)$$

This four-point correlator can further be factorized into two-point correlators in the large c limit as follows

$$S_R^{\text{bdy}}(B_L : B_R) = \lim_{m,n \rightarrow 1} \frac{1}{1-n} \log \frac{\Omega_{Q'}^{2h_{g_A}} \Omega_{P'}^{2h_{g_A}} \langle \sigma_{g_A}(Q') \sigma_{g_A^{-1}}(Q) \rangle_{CFT^{\otimes mn}} \langle \sigma_{g_B}(P') \sigma_{g_B^{-1}}(P) \rangle_{CFT^{\otimes mn}}}{\Omega_{Q'}^{2nh_m} \Omega_{P'}^{2nh_m} \langle \sigma_{g_A}(Q') \sigma_{g_A^{-1}}(Q) \rangle_{CFT^{\otimes m}}^n \langle \sigma_{g_B}(P') \sigma_{g_B^{-1}}(P) \rangle_{CFT^{\otimes m}}^n}. \quad (4.18)$$

It is easy to show that the numerator and the denominator in the above expression cancel out in the limit $n \rightarrow 1$. Thus the reflected entropy vanishes for this phase.

Bulk description

As shown in fig. 15, the entanglement wedges of B_L and B_R are naturally disjoint, as a result there is no EWCS in this configuration. Therefore the holographic generalised

reflected entropy receives contribution only from the defect term, represented by the first term in eq. (2.24). This term can be computed using the BCFT two point correlator of twist operators at Q' and P' , expressed as

$$S_R^{\text{bulk}}(B_L : B_R) = S_R^{\text{eff}} = \lim_{m,n \rightarrow 1} \frac{1}{1-n} \log \frac{\Omega_{Q'}^{2h_{g_A}} \Omega_{P'}^{2h_{g_A}} \langle \sigma_{g_A}(Q') \sigma_{g_B}(P') \rangle_{BCFT^{\otimes mn}}}{\Omega_{Q'}^{2nh_m} \Omega_{P'}^{2nh_m} \langle \sigma_{g_m}(Q') \sigma_{g_m}(P') \rangle_{BCFT^{\otimes m}}^n}. \quad (4.19)$$

Using the doubling trick [15] we may write

$$\langle \sigma_{g_A}(Q') \sigma_{g_B}(P') \rangle_{BCFT} = \langle \sigma_{g_A}(Q') \sigma_{g_A}(Q'') \sigma_{g_B}(P') \sigma_{g_B}(P'') \rangle_{CFT}, \quad (4.20)$$

where P'' and Q'' are symmetric points to P' and Q' respectively. As a result eq. (4.19) is essentially the same as eq. (4.17) in the boundary picture, and therefore the reflected entropy vanishes in the limit $n \rightarrow 1$.

4.3 Reflected entropy between black hole interior and radiation

In this subsection we compute the reflected entropy between the black hole region and radiation region in presence of $T\bar{T}$ deformation in a time dependent $\text{AdS}_3/\text{BCFT}_2$ setup. As illustrated in figs. 16 and 17, the black hole region and the radiation region are described as B_L (denoted once again by the red line) and $R_L = |MQ|$ respectively. Unlike the previous case, we only have one entanglement phase denoted by the RT surface Γ ending on boundary point $M \equiv (\tau'_2, -x'_2, z'_2)$ and brane point O (the dashed green line in figs. 16 and 17). At later stages of the computation we use the approximation that $x'_2 \rightarrow \infty$, assuming that our subsystem extends infinitely to encompass the entirety of the spacetime of the left side. However, within this entanglement entropy phase, there are two possible reflected entropy phases depending on whether reflected entropy islands exist or not. The final reflected entropy between the black hole interior and radiation region is determined by the minimum of these two phases.

4.3.1 The Entanglement entropy phase

For simplicity of computation we start again in the unprimed coordinates. Using transformations detailed in eq. (4.2) the left subsystem $B_L \cup R_L$ now ends at the boundary point $M \equiv (\tau_2, -x_2, z_2)$. In the limit $x'_2 \rightarrow \infty$ this point reduces to $(2, 0, \epsilon)$, where $\epsilon \rightarrow 0$, effectively pushing the endpoint M to spatial infinity. On the other hand, we assume that the Ryu Takayanagi surface Γ intersects at the brane at $O \equiv (y, x_y)$. The computations will follow the same line of arguments as given in [81].

Boundary description

The entanglement entropy in the boundary description may be computed by using the island formula [1–3]. The effective EE (S^{eff}) in the island formula, which for the left subsystem $B_L \cup R_L$ is given by the two point correlator of twist fields at brane point O and boundary point M as

$$S^{\text{eff}}(B_L \cup R_L) = \lim_{m \rightarrow 1} \frac{1}{1-m} \log \left[\Omega_O^{2h_m} \langle \sigma_{g_m^{-1}}(M) \sigma_{g_m}(O) \rangle_{CFT^{\otimes m}} \right], \quad (4.21)$$

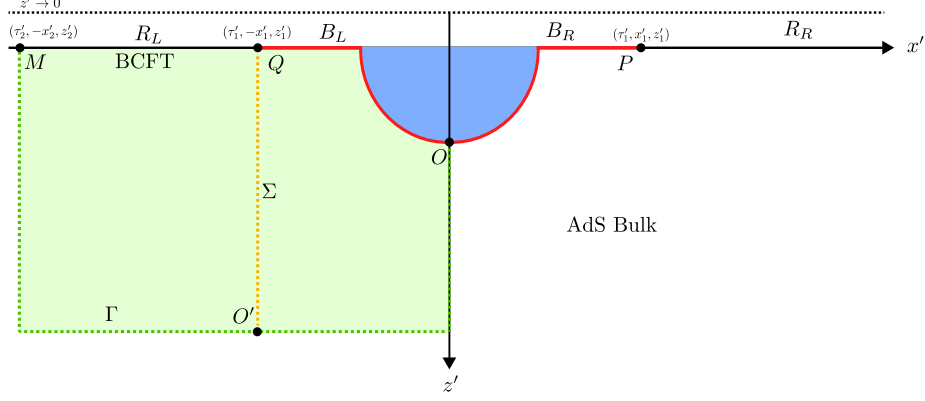


Figure 16: The diagram represents the no-island phase for reflected entropy between radiation and black hole. The green shaded region represents the entanglement wedge for the left system $R_L \cup B_L$, which is separated from the right system by the z axis. The entanglement wedge cross section is represented by the yellow dashed line QO' .

where $h_m = \frac{c}{24} (m - \frac{1}{m})$. Including the area term, which in this scenario retains the same functional form as shown in eq. (3.21), the generalized entanglement entropy can be expressed as

$$S^{\text{gen}}(B_L \cup R_L) = \frac{c}{3} \left(\log \left[\frac{(x_2 + x_y)^2 + (\tau_2 + y)^2}{\epsilon} \right] + \log \left[\frac{\ell}{\epsilon_y (z_2 + y \operatorname{sech} \frac{\sigma_0}{\ell})} \right] + \cosh^{-1} \left[\frac{\sqrt{y^2 + z_2^2 + 2z_2 y \operatorname{sech} \frac{\sigma_0}{\ell}}}{z_2 + y \operatorname{sech} \frac{\sigma_0}{\ell}} \right] \right). \quad (4.22)$$

Extremizing eq. (4.22) for the brane coordinate y , we find that $O \equiv (2, 0)$ in the limit $x'_2 \rightarrow \infty$. Thus the entanglement entropy is

$$S(B_L \cup R_L) = \frac{c}{3} \left(\log \frac{4}{\epsilon} + \log \frac{2\ell}{\epsilon_y \operatorname{sech} \frac{\sigma_0}{\ell}} + \frac{\sigma_0}{\ell} \right). \quad (4.23)$$

Bulk description

In the bulk description, the holographic EE may be written by using eq. (2.10) as

$$S(B_L \cup R_L) = \frac{c}{3} \left(\cosh^{-1} \left[\frac{(x_2 + x_y)^2 + y^2 + 2z_2^2 + \tau_2^2 + 2yz_c \operatorname{sech} \frac{\sigma_0}{\ell} + 2y\tau_2 \tanh \frac{\sigma_0}{\ell}}{2z_2^2 + 2yz_2 \operatorname{sech} \frac{\sigma_0}{\ell}} \right] + \log \left[\frac{2y\ell}{\epsilon_y (z_2 + y \operatorname{sech} \frac{\sigma_0}{\ell})} \right] \right), \quad (4.24)$$

where the first term is the geodesic length of the RT surface Γ and the second term represents the matter defect contribution on the brane, computed in eq. (3.26). Now for the brane coordinate y , eq. (4.24) is extremized (in the limit $x'_2 \rightarrow \infty$) at $y = 2$ and $x_y = 0$. Putting back these values in eq. (4.24), we get the holographic entanglement entropy in the limit $x'_2 \rightarrow \infty$ to be the same as eq. (4.23).

4.3.2 Reflected Entropy Phase: 1

With the endpoints of the left system $B_L \cup R_L$ determined, we can proceed to compute the reflected entropy between subsystems B_L and R_L . As depicted in fig. 16, the EWCS intersects with the surface Γ for the first reflected entropy phase. Consequently, the radiation region R_L does not have any island on the brane, and the entire black hole region on the brane belongs to B_L .

Boundary description

Since the radiation subsystem R_L does not possess any island on the brane, the area term in eq. (2.23) does not contribute to the generalised reflected entropy. As a result, in this phase the reflected entropy between subsystems B_L and R_L is determined by a three point correlation function of brane point O , and boundary points M and Q as

$$S_R^{\text{bdy}}(B_L : R_L) = \lim_{m,n \rightarrow 1} \frac{1}{1-n} \log \frac{\Omega_O^{2h_{g_B}} \langle \sigma_{g_A}(M) \sigma_{g_A^{-1}g_B}(Q) \sigma_{g_B^{-1}}(O) \rangle_{CFT^{\otimes mn}}}{\langle \sigma_{g_m}(M) \sigma_{g_m}(O) \rangle_{CFT^{\otimes m}}^n}. \quad (4.25)$$

In the limit $x'_2 \rightarrow \infty$, the reflected entropy has the form

$$S_R^{\text{bdy}}(B_L : R_L) = \frac{c}{3} \log \left[\frac{\sqrt{x_1^2 + (\tau_1 - 2)^2} \sqrt{x_1^2 + (\tau_1 + 2)^2}}{2z_1} \right] = \frac{c}{3} \log \left[\frac{2}{z_R} \right], \quad (4.26)$$

where in the final step we use eqs. (4.2), (4.4) and (4.6) to express the results in the Rindler coordinates.

Bulk description

In this phase, the radiation region lacks an island on the brane, causing the first term in eq. (2.24) to vanish. Therefore, computing the holographic reflected entropy in this scenario simplifies to evaluating the second term, which is the geodesic length of Σ . The equation of Γ in the limit $x'_2 \rightarrow \infty$ is given by (check appendix A.2 for details)

$$z^2 + \tau^2 = 4. \quad (4.27)$$

Assuming that Σ ends on an arbitrary point on Γ , its length is obtained using eq. (3.1) as

$$\text{Area}[\Sigma] = \cosh^{-1} \left[\frac{4 + x_1^2 - 2\tau\tau_1 + \tau_1^2}{2z_1\sqrt{4 - \tau^2}} \right]. \quad (4.28)$$

Extremizing eq. (4.28) over τ , we get the extremum value of $\tau = \frac{8\tau_1}{4+x_1^2+\tau_1^2}$. Substituting the value of τ in the above expression the reflected entropy in the bulk description matches exactly with the field theory results in eq. (4.26).

4.3.3 Reflected Entropy Phase: 2

The second reflected entropy phase corresponds to the scenario where Σ intersects on the brane, leading to the formation of a radiation island region on the brane. Although the entirety of the island region $Q'P'$ belongs to the radiation subsystem $R_L \cup R_R$, only the portion $Q'O$ belongs to the left radiation subsystem R_L .

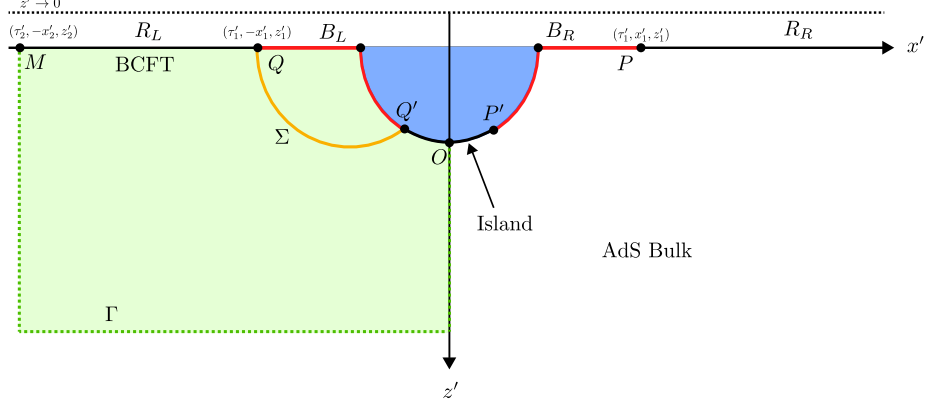


Figure 17: This illustration represents the island phase of reflected entropy between radiation and black hole. The island region (denoted by the black curve $Q'P'$) belongs to the entanglement wedge of radiation, of which the section $Q'O$ belongs to the R_L . The EWCS is given by the yellow line QQ' .

Boundary description

As evident from fig. 17, the effective reflected entropy is given by the two point function of twist operators at the boundary point Q and brane point Q' as

$$S_R^{\text{eff}}(B_L : R_L) = \lim_{m,n \rightarrow 1} \frac{1}{1-n} \log \frac{\Omega_{Q'}^{2h_{g_A g_B^{-1}}} \langle \sigma_{g_A^{-1} g_B}(Q) \sigma_{g_A g_B^{-1}}(Q') \rangle_{CFT^{\otimes mn}}}{\langle \sigma_{g_m}(Q) \sigma_{g_m}(Q') \rangle_{CFT^{\otimes m}}^n}. \quad (4.29)$$

Adding to it the area term eq. (3.21), the generalised reflected entropy eq. (2.23) may be obtained as

$$S_R^{\text{gen}}(B_L : R_L) = \frac{c}{3} \left(\log \frac{(y + \tau_1)^2}{z_1} + \log \frac{\ell}{\epsilon_y(z_1 + y \text{sech} \frac{\sigma_0}{\ell})} \right) + \frac{c}{3} \cosh^{-1} \left[\frac{\sqrt{y^2 + z_1^2 + 2z_1 y \text{sech} \frac{\sigma_0}{\ell}}}{z_1 + y \text{sech} \frac{\sigma_0}{\ell}} \right] \quad (4.30)$$

Extremizing S_R^{gen} over the brane coordinate y up to first order in z_1 , we get $y = \tau_1 - 2z_1 e^{\frac{\sigma_0}{\ell}} + \mathcal{O}(z_1^2)$. This gives the final reflected entropy for this phase as

$$S_R^{\text{bdy}}(B_L : R_L) = \frac{c}{3} \left(\log \frac{2\tau_1}{z_1} + \log \frac{2\ell}{\epsilon_y \text{sech} \frac{\sigma_0}{\ell}} + \frac{\sigma_0}{\ell} \right) - \frac{c}{3} \frac{z_1 e^{\frac{\sigma_0}{\ell}}}{\tau_1} + \mathcal{O}(z_1^2). \quad (4.31)$$

Bulk description

In this scenario, the area term in the generalised reflected entropy eq. (2.24) is simply the length of the EWCS Σ , which may be obtained using eq. (3.21). Including the matter defect term, the generalized reflected entropy is obtained as

$$S_R^{\text{gen}} = \frac{c}{3} \cosh^{-1} \left[\frac{y^2 + 2z_1^2 + \tau_1^2 + 2yz_1 \text{sech} \frac{\sigma_0}{\ell} + 2y\tau_1 \tanh \frac{\sigma_0}{\ell}}{2z_1^2 + 2yz_1 \text{sech} \frac{\sigma_0}{\ell}} \right] + \frac{c}{3} \log \frac{2y\ell}{\epsilon_y(z_1 + y \text{sech} \frac{\sigma_0}{\ell})}. \quad (4.32)$$

Extremizing eq. (4.32) up to first order in z_1 , we have $y_{min} = \tau_1 - 2z_1 e^{\frac{\sigma_0}{\ell}} + \mathcal{O}(z_1^2)$, which gives us

$$\begin{aligned} S_R^{\text{bulk}}(B_L : R_L) &= \frac{c}{3} \left(\log \frac{2\tau_1}{z_1} + \log \frac{2\ell}{\epsilon_y \text{sech} \frac{\sigma_0}{\ell}} + \frac{\sigma_0}{\ell} \right) - \frac{c}{3} \frac{z_1 e^{\frac{\sigma_0}{\ell}}}{\tau_1} + \mathcal{O}(z_1^2) \\ &= \frac{c}{3} \left(\log \frac{2 \sinh X_1}{z_R} + \log \frac{2\ell}{\epsilon_y \text{sech} \frac{\sigma_0}{\ell}} + \frac{\sigma_0}{\ell} \right) - \frac{2c}{3} \frac{z_R e^{\frac{\sigma_0}{\ell}}}{\sinh X_1} + \mathcal{O}(z_R^2), \end{aligned} \quad (4.33)$$

where in the last line we use eqs. (4.2), (4.4) and (4.6) to express the result in Rindler coordinates.

4.4 Reflected entropy between radiation subsystems

In this subsection, we analyse the reflected entropy between the left and right radiation region, described as $R_L = |MQ|$ and $R_R = |PN|$ respectively in fig. 18. In this scenario we encounter two possible EE phases, an island and a no-island phase. Similar to previous subsections, we first perform the computation in unprimed coordinates (Euclidean coordinates) and then transform the result to the Rindler coordinates. The endpoints of R_L are $(\tau_1, -x_1, z_1)$ and $(\tau_2, -x_2, z_2)$, while R_R is defined by endpoints (τ_1, x_1, z_1) and (τ_2, x_2, z_2) .

4.4.1 Entanglement Entropy Phase: 1

In this phase, there are no entanglement entropy islands associated with $R_L \cup R_R$, as illustrated in fig. 18. Consequently the EE may be computed as the sum of the lengths of the two HM surfaces, indicated by the green lines, which may be easily computed using eq. (4.7) as

$$S(R_L \cup R_R) = \frac{2c}{3} \log \frac{2 \cosh T}{z_R}. \quad (4.34)$$

Corresponding to this EE phase, there is only one possible reflected entropy phase between the disjoint radiation subsystems R_L and R_R . The computation of this reflected entropy is detailed as follows.

Boundary description

As seen from the fig. 18, there is no island phase for this EE and reflected entropy for this case, hence the area term in eq. (2.23) does not contribute. Therefore computing the reflected entropy is equivalent to determining the effective reflected entropy between two disjoint intervals R_L and R_R , which is given by the four point correlator of twist fields at boundary points M, Q, P and N as

$$S_R^{\text{bdy}}(R_L : R_R) = \lim_{m, n \rightarrow 1} \frac{1}{1-n} \log \frac{\langle \sigma_{g_A}(Q) \sigma_{g_A^{-1}}(M) \sigma_{g_B}(N) \sigma_{g_B^{-1}}(P) \rangle_{CFT^{\otimes mn}}}{\langle \sigma_{g_m}(Q) \sigma_{g_m}(M) \sigma_{g_m}(N) \sigma_{g_m}(P) \rangle_{CFT^{\otimes m}}^n} = \frac{c}{3} \log \frac{1 + \sqrt{\eta}}{1 - \sqrt{\eta}}, \quad (4.35)$$

where in the second step we have used the four point function in the large central charge limit as provided in [36, 90]. The cross ratio in this case is given as

$$\eta = \frac{(x_2 - x_1)^2 + (\tau_2 - \tau_1)^2}{(x_2 + x_1)^2 + (\tau_2 - \tau_1)^2} = \frac{\sinh^2[\frac{X_2 - X_1}{2}]}{\sinh^2[\frac{X_2 - X_1}{2}] + \cosh^2 T}. \quad (4.36)$$

4.4.2 Entanglement Entropy Phase: 2

In this phase, the presence of entanglement entropy islands corresponding to the radiation regions is observed. In this scenario the EE may be expressed as the sum of the HM surface and two island surfaces (depicted as solid green curves in fig. 19) as,

$$S(R_L \cup R_R) = \frac{c}{3} \left(\frac{\sigma_0}{\ell} + \log \frac{2 \cosh T}{z_R} + \log \frac{2 \sinh X_1}{z_R} + \log \frac{2\ell}{\epsilon_y \operatorname{sech} \frac{\sigma_0}{\ell}} \right) - \frac{c}{3} \frac{z_R e^{\frac{\sigma_0}{\ell}}}{\sinh X_1}, \quad (4.39)$$

where we have made use of eqs. (4.7) and (4.16). In fig. 19, the EE island is depicted as the region $Q'P'$. The brane point O segments the EE island into reflected entropy islands $I_L = |OQ'|$ for subsystem R_L and $I_R = |OP'|$ for subsystem R_R . The computation of reflected entropy in this phase is as follows.

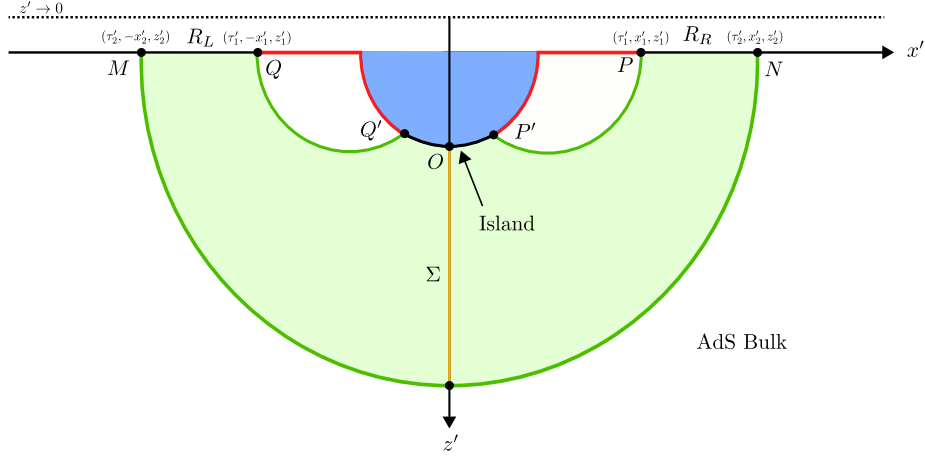


Figure 19: This illustration describes the island phase of EE for the radiation subsystem $R_L \cup R_R$. The entanglement entropy island region is denoted by the black curve $Q'P'$, with point O separating the reflected entropy islands for the radiation subsystems. The yellow line Σ represents the EWCS.

Boundary description

As illustrated from fig. 19, the effective reflected entropy is expressed in terms of a seven-point correlation function involving four boundary points M, Q, P and N , and three brane points Q', P , and O . This correlation function can further be factorized in the large central charge limit into two two-point functions between Q, Q' and P, P' , and a three-point function between M, O and N . Notable, only the three-point correlator contributes, details of

which can be found in [33] as

$$\begin{aligned}
S_R^{\text{eff}} &= \lim_{m,n \rightarrow 1} \frac{1}{1-n} \log \left[\frac{\Omega_{Q'}^{2h_{g_A}} \Omega_O^{2h_{g_{AB}}} \Omega_{P'}^{2h_{g_B}}}{\Omega_{Q'}^{2h_{g_m}} \Omega_{P'}^{2h_{g_m}}} \right. \\
&\quad \times \frac{\langle \sigma_{g_A}(M) \sigma_{g_A^{-1}}(Q) \sigma_{g_A}(Q') \sigma_{g_A^{-1}g_B}(O) \sigma_{g_B^{-1}}(P') \sigma_{g_B}(P) \sigma_{g_B^{-1}}(N) \rangle_{CFT^{\otimes mn}}}{\langle \sigma_{g_m}(M) \sigma_{g_m}(Q) \sigma_{g_m}(Q') \sigma_{g_m}(P') \sigma_{g_m}(P) \sigma_{g_m}(N) \rangle_{CFT^{\otimes m}}^n} \left. \right] \\
&= \lim_{m,n \rightarrow 1} \frac{1}{1-n} \log \frac{\Omega_O^{2h_{g_{AB}}} \langle \sigma_{g_A^{-1}}(Q) \sigma_{g_A}(Q') \rangle_{mn} \langle \sigma_{g_B^{-1}}(P') \sigma_{g_B}(P) \rangle_{mn} \langle \sigma_{g_A}(M) \sigma_{g_A^{-1}g_B}(O) \sigma_{g_B^{-1}}(N) \rangle_{mn}}{\langle \sigma_{g_m}(M) \sigma_{g_m}(N) \rangle_m^n \langle \sigma_{g_m}(Q) \sigma_{g_m}(Q') \rangle_m^n \langle \sigma_{g_m}(P') \sigma_{g_m}(P) \rangle_m^n} \\
&= \lim_{m,n \rightarrow 1} \frac{1}{1-n} \log \frac{\Omega_O^{2h_{g_{AB}}} \langle \sigma_{g_A}(M) \sigma_{g_A^{-1}g_B}(O) \sigma_{g_B^{-1}}(N) \rangle_{mn}}{\langle \sigma_{g_m}(M) \sigma_{g_m}(N) \rangle_m^n}. \tag{4.40}
\end{aligned}$$

Incorporating the area term, the generalized reflected entropy takes the same form as eq. (4.9) with the substitution $x_1 \rightarrow x_2$. Therefore the final reflected entropy for this phase in Rindler coordinates can be directly derived from eq. (4.15) by replacing $X_1 \rightarrow X_2$, yielding the expression

$$\begin{aligned}
S_R^{\text{bdy}}(R_L : R_R) &= \frac{c}{3} \left(\log \left[\frac{\sinh X_2 + \sqrt{\cosh^2 T + \sinh^2 X_2}}{\cosh T} \right] + \log \frac{2\ell}{\epsilon_y \text{sech} \frac{\sigma_0}{\ell}} + \frac{\sigma_0}{\ell} \right) \\
&\quad - \frac{c}{3} \frac{z_R e^{\frac{\sigma_0}{\ell}}}{\sqrt{\cosh^2 T + \sinh^2 X_2}} + \mathcal{O}(z_R^2). \tag{4.41}
\end{aligned}$$

Bulk description

In the bulk description for this phase, the EWCS is represented by the geodesic Σ which connects the HM surface MN to the EOW brane. The geodesic length of Σ can be computed using eq. (3.1). Including the matter defect term, the generalized holographic reflected entropy once again has the same functional form of eq. (4.13) with the substitution $x_1 \rightarrow x_2$. As a result the final holographic reflected entropy in this phase is the same as eq. (4.41).

4.5 Page curve

In this subsection, we describe the Page curves for the reflected entropy for each of the above discussed cases. To plot the Page curve for the reflected entropy, first we need to determine the phase transitions in the EE phases. In presence of $T\bar{T}$ deformation the Page time T_p for the EE phases is given as [81]

$$T_p = \cosh^{-1} \left(\sinh X_1 e^{\frac{\sigma_0}{\ell}} e^{-\frac{z_R e^{\frac{\sigma_0}{\ell}}}{\sinh X_1}} \frac{2\ell}{\epsilon_y \text{sech} \frac{\sigma_0}{\ell}} \right), \tag{4.42}$$

where X_1 is the extent of the black hole interior along the spatial direction, σ_0 is the brane angle, ℓ is the AdS radius, ϵ_y is the UV cutoff on the brane, and z_R denotes the UV cutoff in the Rindler coordinates. Initially no island phase dominates while the island phase, where an EE island appears in the black hole interior, dominates at late times $T > T_p$.

As evident from fig. 20, the Page time T_p exhibits some interesting behavior when plotted against the cut-off z_R and the brane angle σ_0 . Furthermore, it is stimulating

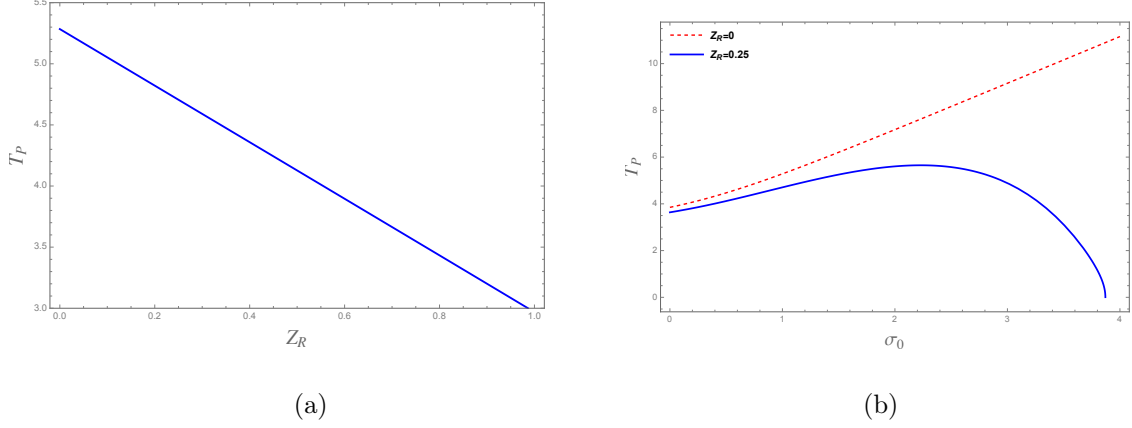


Figure 20: (a) Plot of Page time with cut-off z_R with $X_1 = 1, \epsilon_y = 0.1, \ell = 1$, and $\sigma_0 = 1$. (b) Plot of Page time with brane angle σ_0 with $X_1 = 1, \epsilon_y = 0.1, \ell = 1$, for $z_R = (0, 0.25)$. Though the red dotted line (the curve representing $z_R = 0$) may seem to increase monotonically for all values of σ_0 , it does drop to zero at $\sigma_0 \rightarrow \infty$, where the T_p seems to vanishes.

to note that the Page time drops to zero much more rapidly with σ_0 in presence of $T\bar{T}$ deformation, unlike the scenario with no $T\bar{T}$ deformation where T_p vanishes at $\sigma_0 \rightarrow \infty$. This appears to be correlated with the fact that in the presence of $T\bar{T}$ deformation the asymptotic boundary is no longer at $\sigma \rightarrow \infty$, but pushed inwards to a finite value.

Within the above mentioned EE phases we observe one or more reflected entropy phases depending on the configurations of the subsystems chosen. We now investigate the phase transitions between the various reflected entropy phases, starting with the black hole interior subsystems. We come across two possible EE phases, and within each we observe a single reflected entropy phase. The relevant plots for the reflected entropy between black hole interior subsystems (in units of $c/3$) and time T are given in fig. 21. The first plot shows how the reflected entropy gets modified in presence of $T\bar{T}$ deformation, while the second plot demonstrates how the reflected entropy depends on the brane angle.

For black hole interior and radiation subsystems we observe only one EE phase (as discussed in section 4.3), within which we have two possible reflected entropy phases. As evident from eqs. (4.26) and (4.33), the reflected entropy between black hole interior and radiation for both the phases is independent of time and remains constant for all time. This is expected since no Hartmann-Maldacena surfaces are involved in the computation of the reflected entropy for either phases. As a result, the reflected entropy between black hole interior and radiation subsystems is given by the minimum of the two phases and remains at that constant for all times.

For two radiation subsystems, we once again observe two possible EE phases, and within each we have a single reflected entropy phase. The relevant plots are provided in fig. 22, where we observe the no-island phase dominating at early times and the island phase dominating at late times.

Similar to the reflected entropy between two black hole interior subsystems (fig. 21), the

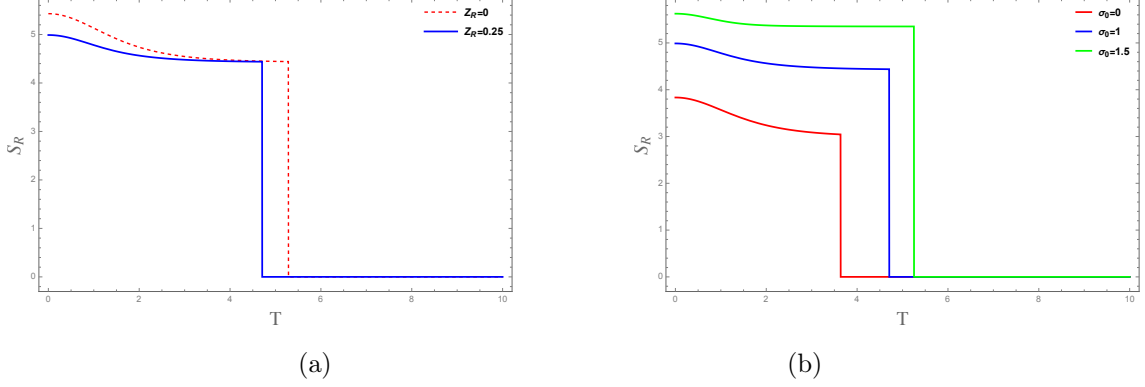


Figure 21: (a) Reflected entropy between black hole interiors with time T in the absence ($z_R = 0$) and presence ($z_R = 0.25$) of $T\bar{T}$ deformation. Here we set $X_1 = 1, \epsilon_y = 0.1, \ell = 1$, and $\sigma_0 = 1$. (b) Reflected entropy between black hole interiors with time T in the presence of $T\bar{T}$ deformation for different brane angle $\sigma_0 = (0, 1, 1.5)$. We have set $X_1 = 1, \epsilon_y = 0.1, \ell = 1$, and $z_R = 0.25$.

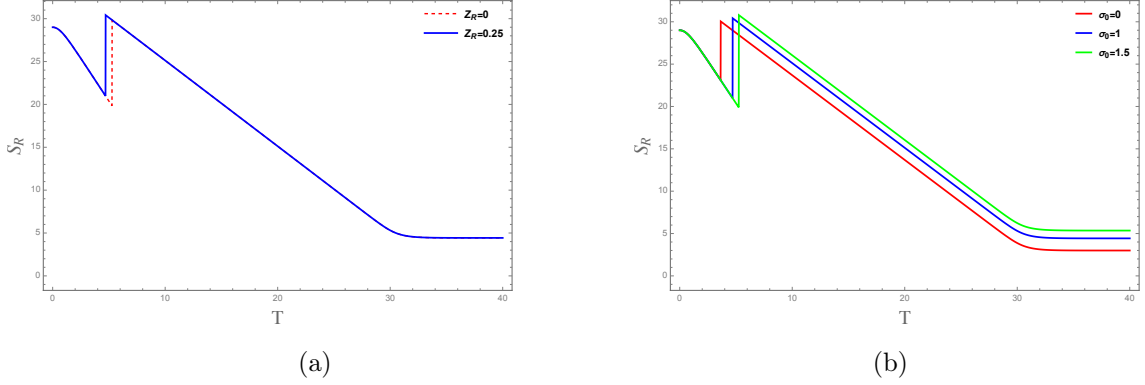


Figure 22: (a) Reflected entropy between left and right intervals of radiation with time T in the absence ($z_R = 0$) and presence ($z_R = 0.25$) of $T\bar{T}$ deformation. Here we set $X_1 = 1, X_2 = 30, \epsilon_y = 0.1, \ell = 1$, and $\sigma_0 = 1$. (b) Reflected entropy between left and right intervals of radiation with time T in the presence of $T\bar{T}$ deformation for different brane angle $\sigma_0 = (0, 1, 1.5)$. We have set $X_1 = 1, X_2 = 30, \epsilon_y = 0.1, \ell = 1$, and $z_R = 0.25$.

reflected entropy between two radiation subsystems (fig. 22) exhibit a sudden discontinuity while transitioning from the no-island to the island phase at the Page time T_p , where it gradually decreases with time and eventually plateaus out. In the limit that the radiation bath extends to spacial infinity $X_2 \rightarrow \infty$, the asymptotic behaviour of the reflected entropy is given by

$$\begin{aligned} \text{Connected Phase : } S_R^{\text{bdy}} &= \frac{c}{3} (X_2 - X_1 - 2 \log \cosh T) \\ \text{Disconnected Phase : } S_R^{\text{bdy}} &= \frac{c}{3} \left(X_2 - \log \cosh T + \log \frac{2\ell}{\epsilon_y \operatorname{sech} \frac{\sigma_0}{\ell}} + \frac{\sigma_0}{\ell} \right). \end{aligned} \quad (4.43)$$

The gap between the reflected entropy at two phases at time of transition T_p in this limit

is

$$S_{\text{gap}} = \frac{c}{3} \left(2 \log \frac{2\ell}{\epsilon_y \operatorname{sech} \frac{\sigma_0}{\ell}} + 2 \frac{\sigma_0}{\ell} + \log(e^{X_1} \sinh X_1) \right) - \frac{c}{3} \frac{z_R e^{\frac{\sigma_0}{\ell}}}{\sinh X_1}. \quad (4.44)$$

5 Conclusions

In this article, we investigate the structure of mixed state entanglement and correlation through the reflected entropy in an AdS_3 braneworld model equipped with a finite distance Dirichlet wall, putatively dual to some boundary conformal field theory with $T\bar{T}$ deformation in the spirit of [50]. In particular, we focus on an AdS_3 geometry characterized by a finite radial cut-off, induced by the $T\bar{T}$ deformation, which is truncated by an end-of-the-world (EOW) brane containing defect matter. As discussed in [81], such a model can naturally arise from a partial reduction, and the resulting braneworld gravity is governed by Neumann boundary conditions on the EOW brane, while we apply AdS/CFT duality for Dirichlet boundary conditions on the finite cut-off surface. In this context, we extend the defect extremal surface (DES) prescription, essentially a double-holographic counterpart to the island formula, for computing the reflected entropy of bipartite mixed states within the defect AdS/BCFT correspondence. The DES formula offers a novel approach to understanding entanglement in such deformed setups, bridging insights from both holographic duality and boundary theories.

We begin by computing the reflected entropy for both adjacent and disjoint intervals in static scenarios, considering various possible entanglement entropy phases. Our findings demonstrate that the results from the DES formula are equivalent to those obtained via the island formula, up to linear orders in the radial cut-off z_c , thereby reinforcing the validity of our approach. We then extend our analysis to time dependent configurations involving an eternal black hole coupled to a radiation bath in the effective lower-dimensional setup. In this context, we compute the reflected entropy between subsystems in the black hole interior, between black hole and radiation subsystems, and between subsystems in the radiation bath utilizing both the island and DES prescriptions. We also examine the time evolution of reflected entropy for these configurations and plot the analogous of the Page curves for the reflected entropy, considering scenarios with and without the $T\bar{T}$ deformation. Once again, we find that the results from boundary and bulk calculations are consistent up to the leading order in the radial cut-off for time-dependent cases, providing a strong consistency check for the proposal discussed earlier.

It is important to note that, as shown in [66, 68, 72] the effects of the $T\bar{T}$ deformation in the boundary theory is captured by modifying the correlation functions by appropriate insertions of stress-tensor components within the framework of conformal perturbation theory. However, in this article, we take a different route and impose that the effects of deformation are encapsulated in the induced metric on the radial cut-off surface, similar to [81]. It will be interesting to explicitly verify the credibility of this approach by developing a perturbation theory for the $T\bar{T}$ -deformed BCFT from scratch.

Although our doubly holographic computations conform to the results from the island formula in the leading order, a critical issue remains to be addressed. Namely, the well-

known breakdown of the holographic proposal in [50] upon the inclusions of bulk conformal matter. A possible way out is to consider the alternative proposal of mixed boundary conditions [53] which can address the presence of matter in the bulk. We leave a critical re-examination of the present work in the context of modified asymptotic boundary conditions for the future.

A potential higher-dimensional extension of the present work, as well as that of [81], possibly in the spirit of [59], warrants further investigation due to the subtleties associated with incorporating conformal matter on the defect brane. Moreover, even in the undeformed case, the DES and island prescriptions do not align consistently in higher dimensions, and the process of partial dimensional reduction necessitates the inclusion of all Kaluza–Klein modes [32]. Resolving these challenges is crucial for developing a robust higher-dimensional framework that accurately captures the effects of $T\bar{T}$ deformations and the dynamics of conformal matter on defect branes.

There are several other future directions to explore. One potential avenue is to investigate the correction to reflected entropy at all orders in the radial cutoff for $T\bar{T}$ deformed BCFT and to verify the equivalence between the island and the DES formula in this scenarios. Furthermore it would be interesting to investigate other mixed state entanglement and correlation measures such as entanglement negativity, odd entanglement entropy, balance partial entanglement and multipartite entanglement in the context of such $T\bar{T}$ deformed BCFT. We leave these interesting open issue for future consideration.

A On geodesics in cut-off AdS_3

A.1 Geodesic on a constant τ -slice

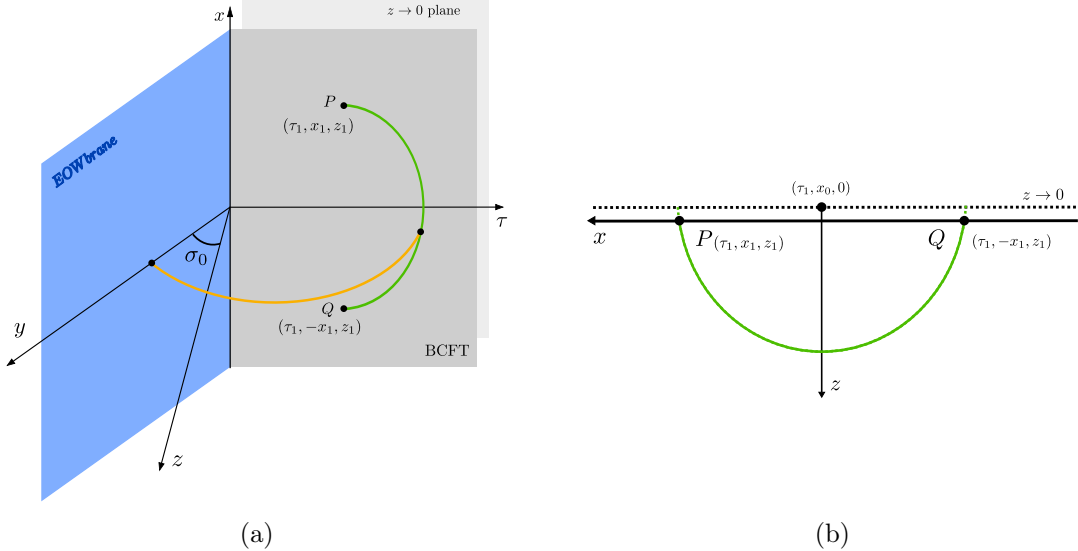


Figure 23: (a) Representation of no-island phase of the entanglement entropy of black hole region in the unprimed coordinates. (b) Schematic for determining the equation of the Hartmann Maldacena surface PQ on a constant τ -slice.

The equation of geodesic in AdS_3 on a constant time slice (as described in fig. 23) is that of a circle given by

$$(x + x_0)^2 + (z - z_0)^2 = R^2, \quad (\text{A.1})$$

where (τ_1, x_0, z_0) is the coordinates of the center and R is the radius of the circle. Given that the circle must be centred at $z_0 = 0$, solving for the points $(\pm x_1, z_1)$, i.e., solving

$$(x_1 + x_0)^2 + z_1^2 = R^2, \quad (x_1 - x_0)^2 + z_1^2 = R^2 \quad (\text{A.2})$$

gives us the $x_0 = 0$ and $R = \sqrt{x_1^2 + z_1^2}$. Considering that the EWCS lands on this Ryu Takayanagi surface at arbitrary value x , this gives us the value of z as

$$z = \sqrt{-x^2 + x_1^2 + z_1^2} \quad (\text{A.3})$$

A.2 Geodesic on a constant x -slice

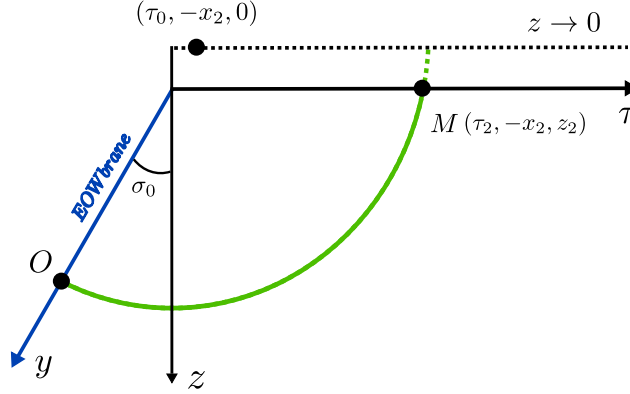


Figure 24: Schematic for determining the equation of the Ryu Takayanagi surface MO on a constant x -slice.

In this case the geodesic in AdS_3 is on a constant x -slice (refer to fig. 24), which is described by the circle

$$(\tau - \tau_0)^2 + (z - z_0)^2 = R^2. \quad (\text{A.4})$$

Here $(\tau_0, -x_2, z_0)$ is the coordinates of the center and R is the radius of the circle. Given that the circle must be centred at $z_0 = 0$, then solving for boundary point $M \equiv (\tau_2, -x_2, z_2)$ and brane point $O \equiv (-\tau_2 \tanh \sigma_0, -x_2, z_2 + \tau_2 \text{sech } \sigma_0)$, i.e., solving

$$z_2^2 + (\tau_2 - \tau_0)^2 = R^2, \quad (z_2 + \tau_2 \text{sech } \frac{\sigma_0}{\ell})^2 + (\tau_0 + \tau_2 \tanh \frac{\sigma_0}{\ell})^2 = R^2 \quad (\text{A.5})$$

gives us

$$R = \sqrt{\frac{2z_2(z_2 + \tau_2 \text{sech } \frac{\sigma_0}{\ell}) + \tau_2^2(1 + \tanh \frac{\sigma_0}{\ell})}{1 + \tanh \frac{\sigma_0}{\ell}}}, \quad \tau_0 = -\frac{z_2 \text{sech } \frac{\sigma_0}{\ell}}{1 + \tanh \frac{\sigma_0}{\ell}}. \quad (\text{A.6})$$

In the limit $x'_2 \rightarrow \infty$ (and by employing eq. (4.2)) it reduces to $R \rightarrow 2$ and $\tau_0 \rightarrow 0$. Thus the equation of the circle in the above mentioned limit is given as

$$z^2 + \tau^2 = 4. \quad (\text{A.7})$$

References

- [1] A. Almheiri, R. Mahajan, J. Maldacena, and Y. Zhao, “The Page curve of Hawking radiation from semiclassical geometry,” *JHEP* **03** (2020) 149, [arXiv:1908.10996 \[hep-th\]](#).
- [2] A. Almheiri, N. Engelhardt, D. Marolf, and H. Maxfield, “The entropy of bulk quantum fields and the entanglement wedge of an evaporating black hole,” *JHEP* **12** (2019) 063, [arXiv:1905.08762 \[hep-th\]](#).
- [3] A. Almheiri, T. Hartman, J. Maldacena, E. Shaghoulian, and A. Tajdini, “Replica Wormholes and the Entropy of Hawking Radiation,” *JHEP* **05** (2020) 013, [arXiv:1911.12333 \[hep-th\]](#).
- [4] A. Almheiri, R. Mahajan, and J. E. Santos, “Entanglement islands in higher dimensions,” *SciPost Phys.* **9** no. 1, (2020) 001, [arXiv:1911.09666 \[hep-th\]](#).
- [5] A. Almheiri, R. Mahajan, and J. Maldacena, “Islands outside the horizon,” [arXiv:1910.11077 \[hep-th\]](#).
- [6] A. Almheiri, T. Hartman, J. Maldacena, E. Shaghoulian, and A. Tajdini, “The entropy of Hawking radiation,” [arXiv:2006.06872 \[hep-th\]](#).
- [7] D. N. Page, “Information in black hole radiation,” *Phys. Rev. Lett.* **71** (1993) 3743–3746, [arXiv:hep-th/9306083](#).
- [8] D. N. Page, “Average entropy of a subsystem,” *Phys. Rev. Lett.* **71** (1993) 1291–1294, [arXiv:gr-qc/9305007](#).
- [9] D. N. Page, “Time Dependence of Hawking Radiation Entropy,” *JCAP* **09** (2013) 028, [arXiv:1301.4995 \[hep-th\]](#).
- [10] N. Engelhardt and A. C. Wall, “Quantum Extremal Surfaces: Holographic Entanglement Entropy beyond the Classical Regime,” *JHEP* **01** (2015) 073, [arXiv:1408.3203 \[hep-th\]](#).
- [11] S. Ryu and T. Takayanagi, “Holographic derivation of entanglement entropy from AdS/CFT,” *Phys. Rev. Lett.* **96** (2006) 181602, [arXiv:hep-th/0603001](#).
- [12] V. E. Hubeny, M. Rangamani, and T. Takayanagi, “A Covariant holographic entanglement entropy proposal,” *JHEP* **07** (2007) 062, [arXiv:0705.0016 \[hep-th\]](#).
- [13] T. Faulkner, A. Lewkowycz, and J. Maldacena, “Quantum corrections to holographic entanglement entropy,” *JHEP* **11** (2013) 074, [arXiv:1307.2892 \[hep-th\]](#).
- [14] H. Geng, “Replica Wormholes and Entanglement Islands in the Karch-Randall Braneworld,” [arXiv:2405.14872 \[hep-th\]](#).
- [15] J. Sully, M. V. Raamsdonk, and D. Wakeham, “BCFT entanglement entropy at large central charge and the black hole interior,” *JHEP* **03** (2021) 167, [arXiv:2004.13088 \[hep-th\]](#).
- [16] M. Rozali, J. Sully, M. Van Raamsdonk, C. Waddell, and D. Wakeham, “Information radiation in BCFT models of black holes,” *JHEP* **05** (2020) 004, [arXiv:1910.12836 \[hep-th\]](#).
- [17] H. Z. Chen, R. C. Myers, D. Neuenfeld, I. A. Reyes, and J. Sandor, “Quantum Extremal Islands Made Easy, Part I: Entanglement on the Brane,” *JHEP* **10** (2020) 166, [arXiv:2006.04851 \[hep-th\]](#).
- [18] H. Z. Chen, R. C. Myers, D. Neuenfeld, I. A. Reyes, and J. Sandor, “Quantum Extremal

- Islands Made Easy, Part II: Black Holes on the Brane,” *JHEP* **12** (2020) 025, [arXiv:2010.00018 \[hep-th\]](#).
- [19] G. Grimaldi, J. Hernandez, and R. C. Myers, “Quantum Extremal Islands Made Easy, Part IV: Massive Black Holes on the Brane,” [arXiv:2202.00679 \[hep-th\]](#).
 - [20] K. Suzuki and T. Takayanagi, “BCFT and Islands in Two Dimensions,” [arXiv:2202.08462 \[hep-th\]](#).
 - [21] H. Geng and A. Karch, “Massive islands,” *JHEP* **09** (2020) 121, [arXiv:2006.02438 \[hep-th\]](#).
 - [22] H. Geng, A. Karch, C. Perez-Pardavila, S. Raju, L. Randall, M. Riojas, and S. Shashi, “Information Transfer with a Gravitating Bath,” *SciPost Phys.* **10** no. 5, (2021) 103, [arXiv:2012.04671 \[hep-th\]](#).
 - [23] H. Geng, S. Lüster, R. K. Mishra, and D. Wakeham, “Holographic BCFTs and Communicating Black Holes,” *jhep* **08** (2021) 003, [arXiv:2104.07039 \[hep-th\]](#).
 - [24] H. Geng, A. Karch, C. Perez-Pardavila, S. Raju, L. Randall, M. Riojas, and S. Shashi, “Entanglement Phase Structure of a Holographic BCFT in a Black Hole Background,” [arXiv:2112.09132 \[hep-th\]](#).
 - [25] H. Geng, A. Karch, C. Perez-Pardavila, S. Raju, L. Randall, M. Riojas, and S. Shashi, “Inconsistency of Islands in Theories with Long-Range Gravity,” [arXiv:2107.03390 \[hep-th\]](#).
 - [26] A. Karch, H. Sun, and C. F. Uhlemann, “Double holography in string theory,” *JHEP* **10** (2022) 012, [arXiv:2206.11292 \[hep-th\]](#).
 - [27] J. L. Cardy, “Boundary conformal field theory,” [arXiv:hep-th/0411189](#).
 - [28] T. Takayanagi, “Holographic Dual of BCFT,” *Phys. Rev. Lett.* **107** (2011) 101602, [arXiv:1105.5165 \[hep-th\]](#).
 - [29] M. Fujita, T. Takayanagi, and E. Tonni, “Aspects of AdS/BCFT,” *JHEP* **11** (2011) 043, [arXiv:1108.5152 \[hep-th\]](#).
 - [30] J. Kastikainen and S. Shashi, “Structure of holographic BCFT correlators from geodesics,” *Phys. Rev. D* **105** no. 4, (2022) 046007, [arXiv:2109.00079 \[hep-th\]](#).
 - [31] F. Deng, J. Chu, and Y. Zhou, “Defect extremal surface as the holographic counterpart of Island formula,” *JHEP* **03** (2021) 008, [arXiv:2012.07612 \[hep-th\]](#).
 - [32] J. Chu, F. Deng, and Y. Zhou, “Page curve from defect extremal surface and island in higher dimensions,” *JHEP* **10** (2021) 149, [arXiv:2105.09106 \[hep-th\]](#).
 - [33] T. Li, M.-K. Yuan, and Y. Zhou, “Defect extremal surface for reflected entropy,” *JHEP* **01** (2022) 018, [arXiv:2108.08544 \[hep-th\]](#).
 - [34] D. Basu, H. Parihar, V. Raj, and G. Sengupta, “Defect extremal surfaces for entanglement negativity,” [arXiv:2205.07905 \[hep-th\]](#).
 - [35] Y. Shao, M.-K. Yuan, and Y. Zhou, “Entanglement negativity and defect extremal surface,” *SciPost Phys. Core* **7** no. 2, (2024) 027, [arXiv:2206.05951 \[hep-th\]](#).
 - [36] S. Dutta and T. Faulkner, “A canonical purification for the entanglement wedge cross-section,” *JHEP* **03** (2021) 178, [arXiv:1905.00577 \[hep-th\]](#).

- [37] C. Akers, T. Faulkner, S. Lin, and P. Rath, “Reflected entropy in random tensor networks,” [arXiv:2112.09122 \[hep-th\]](#).
- [38] G. Vidal and R. F. Werner, “Computable measure of entanglement,” *Phys. Rev. A* **65** (2002) 032314, [arXiv:quant-ph/0102117](#).
- [39] M. B. Plenio, “Logarithmic Negativity: A Full Entanglement Monotone That is not Convex,” *Phys. Rev. Lett.* **95** no. 9, (2005) 090503, [arXiv:quant-ph/0505071](#).
- [40] T. Takayanagi and K. Umemoto, “Entanglement of purification through holographic duality,” *Nature Phys.* **14** no. 6, (2018) 573–577, [arXiv:1708.09393 \[hep-th\]](#).
- [41] P. Nguyen, T. Devakul, M. G. Halbasch, M. P. Zaletel, and B. Swingle, “Entanglement of purification: from spin chains to holography,” *JHEP* **01** (2018) 098, [arXiv:1709.07424 \[hep-th\]](#).
- [42] Q. Wen, “Balanced Partial Entanglement and the Entanglement Wedge Cross Section,” *JHEP* **04** (2021) 301, [arXiv:2103.00415 \[hep-th\]](#).
- [43] T. Li, J. Chu, and Y. Zhou, “Reflected Entropy for an Evaporating Black Hole,” *JHEP* **11** (2020) 155, [arXiv:2006.10846 \[hep-th\]](#).
- [44] V. Chandrasekaran, M. Miyaji, and P. Rath, “Including contributions from entanglement islands to the reflected entropy,” *Phys. Rev. D* **102** no. 8, (2020) 086009, [arXiv:2006.10754 \[hep-th\]](#).
- [45] H.-S. Jeong, K.-Y. Kim, and M. Nishida, “Reflected Entropy and Entanglement Wedge Cross Section with the First Order Correction,” *JHEP* **12** (2019) 170, [arXiv:1909.02806 \[hep-th\]](#).
- [46] J. Kumar Basak, D. Basu, V. Malvimat, H. Parihar, and G. Sengupta, “Islands for entanglement negativity,” *SciPost Phys.* **12** no. 1, (2022) 003, [arXiv:2012.03983 \[hep-th\]](#).
- [47] A. B. Zamolodchikov, “Expectation value of composite field T anti- T in two-dimensional quantum field theory,” [arXiv:hep-th/0401146](#).
- [48] A. Cavaglià, S. Negro, I. M. Szécsényi, and R. Tateo, “ $T\bar{T}$ -deformed 2D Quantum Field Theories,” *JHEP* **10** (2016) 112, [arXiv:1608.05534 \[hep-th\]](#).
- [49] F. A. Smirnov and A. B. Zamolodchikov, “On space of integrable quantum field theories,” *Nucl. Phys. B* **915** (2017) 363–383, [arXiv:1608.05499 \[hep-th\]](#).
- [50] L. McGough, M. Mezei, and H. Verlinde, “Moving the CFT into the bulk with $T\bar{T}$,” *JHEP* **04** (2018) 010, [arXiv:1611.03470 \[hep-th\]](#).
- [51] S. Hirano and M. Shigemori, “Random boundary geometry and gravity dual of $T\bar{T}$ deformation,” *JHEP* **11** (2020) 108, [arXiv:2003.06300 \[hep-th\]](#).
- [52] P. Kraus, J. Liu, and D. Marolf, “Cutoff AdS_3 versus the $T\bar{T}$ deformation,” *JHEP* **07** (2018) 027, [arXiv:1801.02714 \[hep-th\]](#).
- [53] M. Guica and R. Monten, “ $T\bar{T}$ and the mirage of a bulk cutoff,” *SciPost Phys.* **10** no. 2, (2021) 024, [arXiv:1906.11251 \[hep-th\]](#).
- [54] S. Dubovsky, V. Gorbenko, and G. Hernández-Chifflet, “ $T\bar{T}$ partition function from topological gravity,” *JHEP* **09** (2018) 158, [arXiv:1805.07386 \[hep-th\]](#).
- [55] A. J. Tolley, “ $T\bar{T}$ deformations, massive gravity and non-critical strings,” *JHEP* **06** (2020) 050, [arXiv:1911.06142 \[hep-th\]](#).

- [56] V. Shyam, “Background independent holographic dual to $T\bar{T}$ deformed CFT with large central charge in 2 dimensions,” *JHEP* **10** (2017) 108, [arXiv:1707.08118 \[hep-th\]](#).
- [57] W. Cottrell and A. Hashimoto, “Comments on $T\bar{T}$ double trace deformations and boundary conditions,” *Phys. Lett. B* **789** (2019) 251–255, [arXiv:1801.09708 \[hep-th\]](#).
- [58] M. Taylor, “TT deformations in general dimensions,” [arXiv:1805.10287 \[hep-th\]](#).
- [59] T. Hartman, J. Kruthoff, E. Shaghoulian, and A. Tajdini, “Holography at finite cutoff with a T^2 deformation,” *JHEP* **03** (2019) 004, [arXiv:1807.11401 \[hep-th\]](#).
- [60] V. Shyam, “Finite Cutoff AdS_5 Holography and the Generalized Gradient Flow,” *JHEP* **12** (2018) 086, [arXiv:1808.07760 \[hep-th\]](#).
- [61] P. Caputa, S. Datta, and V. Shyam, “Sphere partition functions & cut-off AdS,” *JHEP* **05** (2019) 112, [arXiv:1902.10893 \[hep-th\]](#).
- [62] A. Giveon, N. Itzhaki, and D. Kutasov, “A solvable irrelevant deformation of $\text{AdS}_3/\text{CFT}_2$,” *JHEP* **12** (2017) 155, [arXiv:1707.05800 \[hep-th\]](#).
- [63] M. Asrat, A. Giveon, N. Itzhaki, and D. Kutasov, “Holography Beyond AdS,” *Nucl. Phys. B* **932** (2018) 241–253, [arXiv:1711.02690 \[hep-th\]](#).
- [64] W. Donnelly and V. Shyam, “Entanglement entropy and $T\bar{T}$ deformation,” *Phys. Rev. Lett.* **121** no. 13, (2018) 131602, [arXiv:1806.07444 \[hep-th\]](#).
- [65] A. Lewkowycz, J. Liu, E. Silverstein, and G. Torroba, “ $T\bar{T}$ and EE, with implications for (A)dS subregion encodings,” *JHEP* **04** (2020) 152, [arXiv:1909.13808 \[hep-th\]](#).
- [66] B. Chen, L. Chen, and P.-X. Hao, “Entanglement entropy in $T\bar{T}$ -deformed CFT,” *Phys. Rev. D* **98** no. 8, (2018) 086025, [arXiv:1807.08293 \[hep-th\]](#).
- [67] A. Banerjee, A. Bhattacharyya, and S. Chakraborty, “Entanglement Entropy for TT deformed CFT in general dimensions,” *Nucl. Phys. B* **948** (2019) 114775, [arXiv:1904.00716 \[hep-th\]](#).
- [68] H.-S. Jeong, K.-Y. Kim, and M. Nishida, “Entanglement and Rényi entropy of multiple intervals in $T\bar{T}$ -deformed CFT and holography,” *Phys. Rev. D* **100** no. 10, (2019) 106015, [arXiv:1906.03894 \[hep-th\]](#).
- [69] C. Murdia, Y. Nomura, P. Rath, and N. Salzetta, “Comments on holographic entanglement entropy in TT deformed conformal field theories,” *Phys. Rev. D* **100** no. 2, (2019) 026011, [arXiv:1904.04408 \[hep-th\]](#).
- [70] C. Park, “Holographic Entanglement Entropy in Cutoff AdS,” *Int. J. Mod. Phys. A* **33** no. 36, (2019) 1850226, [arXiv:1812.00545 \[hep-th\]](#).
- [71] M. Asrat, “Entropic c -functions in $T\bar{T}$, $J\bar{T}$, $T\bar{J}$ deformations,” *Nucl. Phys. B* **960** (2020) 115186, [arXiv:1911.04618 \[hep-th\]](#).
- [72] S. He and H. Shu, “Correlation functions, entanglement and chaos in the $T\bar{T}/J\bar{T}$ -deformed CFTs,” *JHEP* **02** (2020) 088, [arXiv:1907.12603 \[hep-th\]](#).
- [73] S. Griener, “Entanglement entropy and $T\bar{T}$ deformations beyond antipodal points from holography,” *JHEP* **11** (2019) 171, [arXiv:1908.10372 \[hep-th\]](#).
- [74] S. Khoeini-Moghaddam, F. Omid, and C. Paul, “Aspects of Hyperscaling Violating Geometries at Finite Cutoff,” *JHEP* **02** (2021) 121, [arXiv:2011.00305 \[hep-th\]](#).

- [75] D. Basu and V. Raj, “Reflected entropy and timelike entanglement in $T\bar{T}$ deformed CFT_{2S} ,” [arXiv:2402.07253 \[hep-th\]](#).
- [76] D. Basu, S. Biswas, A. Dey, B. Paul, and G. Sengupta, “Odd entanglement entropy in $T\bar{T}$ deformed CFT_2 s and holography,” *Phys. Rev. D* **108** no. 12, (2023) 126013, [arXiv:2307.04832 \[hep-th\]](#).
- [77] D. Basu, Lavish, and B. Paul, “Entanglement negativity in $T\bar{T}$ -deformed CFT_{2S} ,” *Phys. Rev. D* **107** no. 12, (2023) 126026, [arXiv:2302.11435 \[hep-th\]](#).
- [78] D. Basu and S. Biswas, “Entanglement, $T\bar{T}$ and rotating black holes,” [arXiv:2410.06363 \[hep-th\]](#).
- [79] S. Grieninger, K. Ikeda, and D. E. Kharzeev, “Temporal entanglement entropy as a probe of renormalization group flow,” *JHEP* **05** (2024) 030, [arXiv:2312.08534 \[hep-th\]](#).
- [80] J.-C. Chang, S. He, Y.-X. Liu, and L. Zhao, “The holographic $T\bar{T}$ deformation of the entanglement entropy in (A)dS₃/ CFT_2 ,” [arXiv:2409.08198 \[hep-th\]](#).
- [81] F. Deng, Z. Wang, and Y. Zhou, “End of the world brane meets $T\bar{T}$,” *JHEP* **07** (2024) 036, [arXiv:2310.15031 \[hep-th\]](#).
- [82] F. Deng and Z. Wang, “Holographic boundary conformal field theory with $T\bar{T}$ deformation,” [arXiv:2411.06345 \[hep-th\]](#).
- [83] O. Aharony, D. Marolf, and M. Rangamani, “Conformal field theories in anti-de Sitter space,” *JHEP* **02** (2011) 041, [arXiv:1011.6144 \[hep-th\]](#).
- [84] A. Karch and L. Randall, “Locally localized gravity,” *JHEP* **05** (2001) 008, [arXiv:hep-th/0011156](#).
- [85] L. Randall and R. Sundrum, “An Alternative to compactification,” *Phys. Rev. Lett.* **83** (1999) 4690–4693, [arXiv:hep-th/9906064](#).
- [86] J. M. Maldacena, “The Large N limit of superconformal field theories and supergravity,” *Adv. Theor. Math. Phys.* **2** (1998) 231–252, [arXiv:hep-th/9711200](#).
- [87] J. D. Brown and M. Henneaux, “Central Charges in the Canonical Realization of Asymptotic Symmetries: An Example from Three-Dimensional Gravity,” *Commun. Math. Phys.* **104** (1986) 207–226.
- [88] Y. Kusuki and K. Tamaoka, “Entanglement Wedge Cross Section from CFT: Dynamics of Local Operator Quench,” *JHEP* **02** (2020) 017, [arXiv:1909.06790 \[hep-th\]](#).
- [89] C. Akers, T. Faulkner, S. Lin, and P. Rath, “The Page Curve for Reflected Entropy,” [arXiv:2201.11730 \[hep-th\]](#).
- [90] A. L. Fitzpatrick, J. Kaplan, and M. T. Walters, “Universality of Long-Distance AdS Physics from the CFT Bootstrap,” *JHEP* **08** (2014) 145, [arXiv:1403.6829 \[hep-th\]](#).
- [91] T. Hartman and J. Maldacena, “Time Evolution of Entanglement Entropy from Black Hole Interiors,” *JHEP* **05** (2013) 014, [arXiv:1303.1080 \[hep-th\]](#).